International Journal of Biological Macromolecules 125 (2019) 1275–1288

Contents lists available at ScienceDirect

International Journal of Biological Macromolecules

journal homepage: http://www.elsevier.com/locate/ijbiomac

Phosphorylation compromises FAD binding and intracellular stability of wild-type and cancer-associated NQO1: Insights into flavo-proteome stability

Encarnación Medina-Carmona [a,1], Bruno Rizzuti [b,1], Rubén Martín-Escolano [c], Juan Luis Pacheco-García [a], Noel Mesa-Torres [a], José L. Neira [d,e], Rita Guzzi [b,f], Angel L. Pey [a,*]

[a] Department of Physical Chemistry, University of Granada, 18071 Granada, Spain
[b] CNR-NANOTEC, Licryl-UOS Cosenza and CEMIF.Cal, Department of Physics, University of Calabria, 87036 Rende, Italy
[c] Department of Parasitology, Instituto de Investigación Biosanitaria (ibs.Granada), Hospitales Universitarios De Granada/University of Granada, 18071 Granada, Spain
[d] Instituto de Biología Molecular y Celular, Universidad Miguel Hernández, Avda. del Ferrocarril s/n, 03202 Elche, Alicante, Spain
[e] Instituto de Biocomputación y Física de los Sistemas Complejos (BIFI), 50009 Zaragoza, Spain
[f] Molecular Biophysics Laboratory, Department of Physics, University of Calabria, 87036 Rende, Italy

ARTICLE INFO

Article history:
Received 13 July 2018
Received in revised form 30 August 2018
Accepted 18 September 2018
Available online 19 September 2018

Keywords:
Flavoprotein
Protein phosphorylation
Conformational disease

ABSTRACT

Over a quarter million of protein phosphorylation sites have been identified so far, although the effects of site-specific phosphorylation on protein function and stability, as well as their possible impact in the phenotypic manifestation in genetic diseases are vastly unknown. We investigated here the effects of phosphorylating S82 in human NADP(H):quinone oxidoreductase 1, a representative example of disease-associated flavoprotein in which protein stability is coupled to the intracellular flavin levels. Additionally, the cancer-associated P187S polymorphism causes inactivation and destabilization of the enzyme. By using extensive in vitro and in silico characterization of phosphomimetic S82D mutations, we showed that S82D locally affected the flavin binding site of the wild-type (WT) and P187S proteins thus altering flavin binding affinity, conformational stability and aggregation propensity. Consequently, the phosphomimetic S82D may destabilize the WT protein intracellularly by promoting the formation of the degradation-prone apo-protein. Noteworthy, WT and P187S proteins respond differently to the phosphomimetic mutation in terms of intracellular stability, further supporting differences in molecular recognition of these two variants by the proteasomal degradation pathway. We propose that phosphorylation could have critical consequences on stability and function of human flavoproteins, important for our understanding of genotype-phenotype relationships in their related genetic diseases.

1. Introduction

Post-translational modifications (PTMs) are key factors contributing to modulate the relationships between genotype and phenotype, both in health and in disease [1]. Advances in mass spectrometry and big data analyses at proteomic scale are revealing a colossal amount of sites involved in PTMs [1–3]. Consequently, one of the challenges ahead is to decipher the effects of these PTMs on protein function in a context-dependent manner (protein targets, enzymes involved in the modification or its removal, cellular context, etc. [2,3]). For illustration, the Phosphosite Plus® web site (https://www.phosphosite.org/; [2]) had compiled evidence (by the first quarter of 2018) of about 20,300 non-redundant mammalian proteins that undergo PTMs (up to 415,000 sites), about 69% of them corresponding to phosphorylation of S, T and Y residues. Remarkably, <5% of these sites have been investigated in a site-specific manner. These statistics clearly illustrate the amount of knowledge still lacking for assessing the effects of PTMs on protein function and stability.

The human flavoproteome contains about 90 different proteins that utilize FAD (flavin adenine dinucleotide) or FMN (flavin mononucleotide), both synthesized from dietary riboflavin, mostly to carry out redox reactions [4]. Their key metabolic roles are highlighted by the finding that about 60% of known human flavoproteins are associated to inherited diseases [4]. Therefore, an adequate supply of the flavin precursor riboflavin (also known as vitamin B2) seems fundamental for the function of flavoproteins and to prevent their dysfunction in disease. Remarkably, recent proteome-wide analyses have demonstrated that riboflavin supply is also critical for flavoproteome stability, supporting a

* Corresponding author.
E-mail address: angelpey@ugr.es (A.L. Pey).
[1] These authors equally contributed to this work.

https://doi.org/10.1016/j.ijbiomac.2018.09.108
0141-8130/

link between enhanced intracellular turnover of human flavoproteins and the ubiquitinylation of (flavin-free) apo-proteins [5]. Unfortunately, a deep and general understanding on the structural and dynamic features of human apo-flavoproteins promoting their proteasomal degradation intracellularly, as well as the roles of flavin binding in modulating these features, are often hampered by the difficulty of preparing these apo-proteins *in vitro* as stable forms for detailed analyses. Noteworthy, a recent work has proposed an intriguing mechanism by which newly synthesized FAD (the cofactor utilized by 75% of human flavoproteins; [4]) in human cells due to the catalytic action of FAD synthase (EC 2.7.7.2) can be directly channeled to two different apo-flavoproteins [6,7], although the impact of this process on the stability and function of the human flavoproteome remains largely unexplored.

To provide a current perspective on the effects of phosphorylation on the function and stability of human flavoproteins, we initially mined the PhosphoSite Plus® database (Fig. 1). In this database, we found information for ninety-one human flavoproteins (among those comprehensively reviewed by [4]). Of them, 95.6% contained active phosphorylation sites (Fig. 1A), and 89.6% were known to be multi-phosphorylated (Fig. 1B). Importantly, out of 886 active phosphorylation sites, only 40 have been characterized by site-specific methods or LTPs (about 4.5%; Fig. 1C). This highlights that the impact of phosphorylation on the function and stability of human flavoproteins is largely unknown. Accordingly, for 80% of the phosphorylatable human flavoproteins, no information was available for the effects of phosphorylation at any site (Fig. 1D). For the 40 sites characterized by LTPs *in vitro* and *in cellulo*, phosphorylation had remarkable effects on protein activity (i.e. activation, inhibition, degree of uncoupling, allosteric regulation, protein dynamics…) [8–22] and stability [21–26]. Furthermore, phosphorylation at these sites was shown to modulate a variety of physiopathological processes, including mitochondrial respiration efficiency and production of reactive oxygen species, Alzheimer's disease and cancer [8–11,19,20,24,27–32]. Remarkably, and to the best of our knowledge, no studies have addressed quantitatively the relationship between site-specific phosphorylation and flavin binding affinity, which, in principle, would strongly influence the existing linkage between flavin binding and flavoproteome stability *in vivo* [5].

To investigate the effects of phosphorylation on the genotype-phenotype relationships exhibited by a human flavoprotein in health and disease, we have used in this work the cancer-associated NADP(H):quinone oxidoreductase 1 (NQO1; EC 1.6.5.2) as a model. NQO1 is a stress-inducible and multifunctional protein, involved in the two-electron reduction and detoxification of quinones, bioactivation of cancer pro-drugs, maintenance of antioxidant pools in the reduced state, superoxide scavenging, NAD^+/NADH redox balance, regulatory protein:protein and protein:RNA interactions and 20S proteasome inhibition, among others [33–42]. Alterations in NQO1 expression, stability and function are associated to different extents with a variety of pathologies, including cancer [39,40,43], Parkinson's and Alzheimer's diseases [5,44] and sensitivity towards benzene toxicity [45]. NQO1 forms active dimers containing two functional domains: a N-terminal domain (NTD; residues 1–224), which contains a tightly bound FAD molecule, and a C-terminal domain (CTD; residues 225–274) that stabilizes the dimer and is critical for binding the NADH coenzyme and the substrate [40,46–50]. Upon removal of FAD, apo-NQO1 remains dimeric but shows an expanded conformation with enhanced dynamics and decreased stability compared to those of holo-NQO1 [47,51–54]. The apo-state of NQO1 is efficiently ubiquitinylated in the dynamic CTD leading to its fast proteasomal degradation, which is prevented upon FAD binding (i.e. in the holo-state) [5,55]. Consequently, NQO1 intracellular stability is strongly sensitive to riboflavin starvation but mildly to its supplementation above *normal* levels due to its high affinity for FAD [5,53]. In addition, a common polyporphism in NQO1 (rs1800566/c.C609T/p.P187S) has received substantial attention for several reasons. Originally, its presence in certain tumour cell lines was found to strongly decrease NQO1 protein levels and activity [56,57]. The former effect was due to accelerated proteasomal degradation [57], which was linked to the partial unfolding of the CTD and its efficient ubiquitinylation even in the holo-state [5,47,51,53,58]. The latter primarily originated from enhanced dynamics of the FAD binding site in the apo-state, which decreased by 10- to 100-fold its affinity for the flavin [47,52,58]. These alterations in the FAD binding site of P187S were partially overcome by an evolutionary divergent suppressor mutation (H80R) that developed favourable electrostatic interactions with two neighbouring and

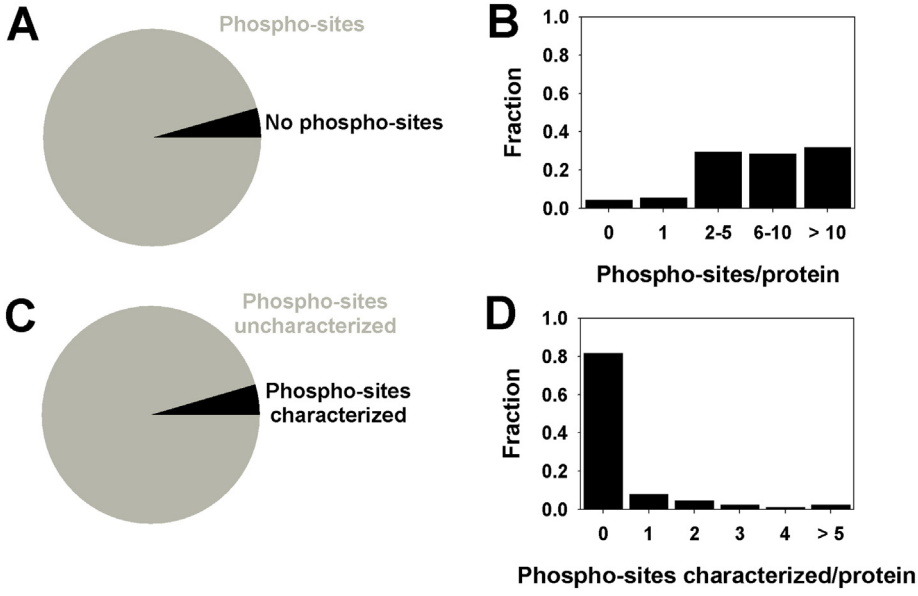

Fig. 1. Most human flavoproteins can be multi-phosphorylated with unknown consequences. A–B) Fraction of human flavoproteins ($N = 91$) for which phosphorylation sites have been identified by high-throughput procedures (HTPs). In panel B, human flavoproteins were clustered in groups according to the number of phosphorylation sites identified per protein by HTPs. C–D) Fraction of phosphorylation sites characterized by site-specific methods (LTPs) out of the set of 886 sites identified by HTPs in 87 different human flavoproteins (C). For this set, in panel D, human flavoproteins were grouped according to the number of phosphorylation sites characterized per protein by LTPs. Analyses were performed using data retrieved from PhosphoSite Plus® [2].

conserved acidic residues (E71 and E78) leading to the functional rescue of P187S *in vitro* and in cultured cells [52,58].

In this work, we investigated the effects of the phosphomimetic mutation S82D on the wild-type (WT) and P187S NQO1. We showed that FAD binding to both WT and P187S is strongly reduced by this phosphomimetic mutation, through local changes in structure and dynamics of the flavin binding site. These alterations in FAD binding may also affect the intracellularly stability of WT, but not that of P187S, highlighting the different response of these two variants regarding ubiquitin-dependent proteasomal degradation coupled to FAD binding. Our results indicate that phosphorylation can strongly affect genotype-phenotype relationships in cancer-associated NQO1 variants, with more general implications for our understanding of these relationships in loss-of-function genetic diseases, and particularly in those affecting human flavoproteins.

2. Materials and methods

2.1. Bioinformatic analyses

Phosphorylation sites for S, T and Y amino acids among human flavoproteins were retrieved from PhosphoSite Plus® (https://www.phosphosite.org) using ninety-one flavoproteins (including isoforms) compiled by [4]. This online tool provided references for those sites identified only by large-scale proteomic procedures (HTPs) and those identified/characterized by site-specific procedures (LTPs).

Analyses of protein kinase A (PKA) phosphorylation sites among mammalian NQO1 sequences was performed using the predictor pkaPS (http://mendel.imp.ac.at/pkaPS/; [59]). Values of pkaPS score were considered as "good hits" if they were above 0, while those between −0.5 and 0 were considered to be "potential hits".

2.2. Modeling of phosphorylation, protein solvent accessibility and structure-based energetic calculations

Changes in thermodynamic stability (i.e. unfolding free energy) were calculated for the apo-proteins using the FoldX force field [60] and the three dimensional structure of WT NQO1 (PDB 2F1O). The FoldX algorithm was used as a plug-in in Yasara molecular graphics, modeling and simulation software [61]. Calculations were performed after energy minimization of the structures and consequent *in silico* mutagenesis and modeling, considering as reference for stability the WT protein at 298 K, 0.1 M ionic strength and pH 7. Solvent accessibilities (as the fraction of the ASA, (solvent) accessible surface area, considering backbone + side-chain) were determined using GETAREA [62].

2.3. Protein expression and purification from E. coli

Site-directed mutagenesis to S82D or S82A was carried out on the pET46 Ek/LIC containing NQO1 sequences earlier described [51,58] and using the QuickChange lightening kit (Agilent Technologies, Madrid, Spain) following standard protocols. Mutagenesis was confirmed by DNA sequencing. This construct allows one to produce the NQO1 with the N-terminal tag containing a hexa-histidine peptide for affinity chromatography purification. It must be noted that this type of N-terminal tag does not seem to cause noticeable effects on the overall structure [47,58,63], specific activity [64], thermal stability and stabilizing effect of FAD [35,51] and the effects of P187S on protein stability and FAD binding [35,46,53,64]. Protein expression and purification was carried out as described [51,65] with some modifications. *E. coli* BL21(DE3) cells were transformed with the corresponding plasmid and grown overnight in 120 mL LBA (LB + 0.1 $mg \cdot ml^{-1}$ ampicillin) at 37 °C. These cultures were diluted in 2.4 L of LBA and grown at 37 °C to an optical density of 0.6 at 600 nm, and then expression was induced by adding 0.5 mM IPTG (isopropyl β-D-1-thiogalactopyranoside). Cells were grown for 6 h at 25 °C, harvested by centrifugation, washed with *binding buffer* (BB, 20 mM sodium phosphate, 300 mM NaCl and 50 mM imidazole at pH 7.4) and frozen overnight at −80 °C. Cells were thawn, resuspended in 60 mL of BB containing EDTA-free protease inhibitor cocktail (Roche) and lysed by sonication. After 20 min of centrifugation at 20000 *g* and 4 °C, supernatants were filtered (through 0.45 μm pore) and loaded into at 4 °C immobilized metal affinity chromatography (IMAC) columns (His Gravitrap™, GE Healthcare) equilibrated in BB. Columns were washed with 50 volumes of BB and proteins eluted with *elution buffer* (EB, BB containing 500 mM imidazole). These eluates were exchanged to 50 mM K-HEPES (2-[4-(2-hydroxyethyl)piperazin-1-yl]ethanesulfonic acid, potassium salt) pH 7.4 using PD-10 columns (GE Healthcare), centrifuged for 30 min at 20000 *g* and 4 °C and the UV–visible spectra were registered in a HP8453 UV–Visible diode-array spectrophotomer (Agilent). These samples from IMAC purification were of high purity (Fig. S1) and activity (Fig. S2) in all cases. These samples were stored at −80 °C after flash freezing in liquid nitrogen. To obtain apo-proteins, NQO1 proteins from IMAC purification were subjected to a size-exclusion chromatography step using a HiLoad® 16/600 Superdex® 200 prep grade (GE Healthcare) and 20 mM K-HEPES 200 mM NaCl at pH 7.4 as mobile phase. Fractions corresponding to the NQO1 dimer were pooled, concentrated to 0.5 mL (using centrifugal concentrators VIVASPIN®6, 30,000 MWCO PES, Sartorius) and treated with 10 mL of *stripping buffer* [SB, BB containing 2 M urea and 2 M KBr, 1 mM DTT (1,4-dithiothreitol) and 1 mM PMSF] at 4 °C for 10 min. These solutions were loaded into IMAC columns at 4 °C equilibrated in SB, washed with 30 volumes of SB, then with 30 volumes of BB and eluted with EB. Samples were immediately exchanged to 50 mM K-HEPES at pH 7.4 using PD-10 columns at 4 °C and concentrated. These *apo-proteins* were of high purity (Fig. S1), contained very low levels of FAD (<0.01 molecules of FAD/NQO1 monomer, based on the A_{450}/A_{280} ratio) and were stored at −80 °C after flash freezing in liquid nitrogen. To obtain *holo-proteins*, apo-proteins were prepared with an appropriate excess of FAD and subsequent analyses were carried out without removing the excess of FAD (note that to preserve the protein as holo-protein a significantly high concentration of *free ligand* is required, particularly for those variants with low affinity for FAD) and including controls with FAD (and without the protein) when needed.

2.4. FAD content in purified NQO1 proteins

FAD content in freshly purified proteins was determined from UV–visible spectra using the experimental A_{450}/A_{280} in 50 mM K-HEPES at pH 7.4 and 25 °C as described [58]. Spectra were acquired in a HP 8453 UV–Visible diode-array spectrophotometer (Agilent).

2.5. Binding affinity for FAD

Binding affinities were customarily studied by fluorescence titrations of apo-proteins with FAD. These experiments were carried out in a Cary Eclipse spectrofluorimeter (Varian). Apo-proteins (0.2 μM) were incubated with 0–10 μM FAD in 50 mM K-HEPES at pH 7.4 and 25 °C as described [58]. Fluorescence emission intensity (exc. 280 nm; em. 340 nm; 5 nm slits) vs. total FAD concentration profiles were acquired in 1 cm path-length cuvettes and fitted to a 1:1 binding model [58]. To provide convergence, the fluorescence emission of the holo-state of P187S/S82D was fixed to half of the apo-state fluorescence since the average fractional quenching value for the rest of variants from this work and from those previously reported in [58] was 0.50 ± 0.06.

For P187S/S82D, which exhibited very low binding affinities for FAD, titrations were also carried out using Near-UV circular dichroism (CD) spectroscopy. Spectra were collected in a Jasco J-710 spectropolarimeter at 25 °C in K-HEPES 50 mM pH 7.4 using 20 μM (in monomer) of apo-protein in the absence or presence of FAD (0–69 μM). Spectra were collected in the 300–600 nm range, at 200 $nm \cdot min^{-1}$, using 2 nm bandwidth, 2 s time reponse and 5 mm path-length cuvettes. Each

spectrum was the average of five scans, and each sample was appropriately corrected for blanks containing the buffer and the corresponding FAD concentration.

2.6. Thermal denaturation

Thermal denaturation of NQO1 proteins, as apo- or holo-proteins (2 μM apo-monomer ±20 μM FAD) was monitored by following changes in tryptophan emission fluorescence in K-HEPES 50 mM at pH 7.4 as recently described [58]. T_m values were reported as mean ± s.d. of three independent measurements.

2.7. Partial proteolysis

Proteolysis kinetics by thermolysin were performed in 50 mM K-HEPES, 10 mM $CaCl_2$, at pH 7.4 and 25 °C as recently described [53,58]. Apo-NQO1 enzymes were used at 10–20 μM concentration, with or without 100 μM FAD, and experiments were typically carried out using 5 nM thermolysin except for holo-WT and holo-S82D (200 nM thermolysin). Samples were analyzed in SDS-PAGE gels (12% acrylamide) and stained with Coomassie® Brilliant blue R250 (Sigma-Aldrich). The intensity of the bands was quantified using ImageJ (https://imagej.nih.gov/ij/). Experiments were performed three times, and the time-dependent decay of uncleaved NQO1 was used to determine first-order rate constants from exponential functions. Second-order rate constants (k_{prot}) were obtained by dividing first-order rate constants by the protease concentration used.

2.8. Far-UV circular dichroism (CD) spectroscopy

Far-UV CD spectroscopy was performed at 25 °C in K-phosphate 20 mM at pH 7.4 using 5 μM (in monomer) of apo-proteins with or without 100 μM FAD. Spectra were collected in a Jasco J-710 spectropolarimeter in the 190–260 nm range, at 100 nm·min^{-1}, using 1 nm bandwidth, 1 s response time and 1 mm path length cuvettes. Each spectrum was the average of four scans, and each sample was prepared in triplicate. Blanks containing buffer (with or without FAD) were also measured under the same experimental conditions and appropriately subtracted. To calculate mean residue ellipticities ($[\Theta]_{MRW}$), we used the following equation:

$$[\Theta]_{MRW} = \frac{MRW \cdot \Theta_{obs}}{10 \cdot l \cdot c}$$

where MRW was equal to the molecular weight of the NQO1 monomer (30,868 g·mol^{-1}) divided by (N-1), being $N = 274$ the number of residues in the monomer, Θ_{obs} was the ellipticity (in deg), l was the path length (in cm) and c the concentration of protein in g·mL^{-1}. Spectra were reported as mean ± s.d. from three replicates.

2.9. Dynamic light scattering (DLS)

DLS was measured at 25 °C in a DynaPro MSX instrument (Wyatt) using 1.5 mm path length cuvettes and 5 μM apo-protein (monomer), in K-phosphate 20 mM at pH 7.4 and in the absence or presence of 100 μM FAD. Twenty spectra were acquired for each DLS analysis, averaged and used to determine the hydrodynamic radius assuming spherical scattering particles (using the Stokes-Einstein approach). Data were reported as mean ± s.d. from three replicates.

2.10. Thiol-modification kinetics

Thiol-modification kinetics of C180 in NQO1 samples was monitored by measuring the changes in A_{412nm} using 5,5′-dithio-bis-[2-nitrobenzoic acid] (DTNB). Experiments were performed in K-HEPES 50 mM, pH 7.4 at 25 °C in a HP 8453 UV–Visible diode-array spectrophotometer (Agilent). Samples were incubated for 5 min in 1 cm cuvettes containing routinely 10 μM NQO1 in protein monomer with or without FAD 50 μM. The reaction was initiated by adding DTNB to a final concentration of 1 mM unless otherwise indicated. The kinetics of DTNB reaction with free *L*-Cys was determined using 2 μM of the amino acid and 10–50 μM of DTNB under the same conditions. The amount of reactive C180 in NQO1 samples was determined upon subtraction of blanks without protein and after 1 h reaction with DTNB, using a $\varepsilon_{412} = 14{,}105\ M^{-1}\cdot cm^{-1}$ and normalized by protein monomer. Reaction kinetics was determined under pseudo first-order conditions (excess of DTNB) by fitting the time dependence of A_{412nm} to a single exponential function to yield pseudo first-order rate constants. The second-order rate constants were determined from the linear dependence of pseudo first-order rate constants on DTNB concentration.

2.11. Aggregation kinetics

Aggregation kinetics was monitored following changes in A_{320nm} using a HP 8453 UV–Visible diode-array spectrophotometer (Agilent). 900 μL of K-HEPES 50 mM at pH 7.4 was preincubated at 37 °C inside quartz cuvettes for 10 min and then 100 μL of protein samples (20 μM apo-protein, in the absence or presence of 200 μM FAD) were diluted into the buffer and manually mixed. A_{320nm} was registered for 80–85 min. Control experiments containing only buffer (with or without a final concentration of 20 μM FAD) were routinely performed to assess background stability. Maximal aggregation rates were determined from first-derivative analyses of the time-dependent A_{320}.

2.12. Interaction of NQO1 with the sterile alpha motif of p73α (SAMp73α)

The interaction of SAMp73α with purified NQO1 proteins was investigated by nuclear magnetic resonance (NMR) spectroscopy. ^{15}N-labelled SAMp73α was produced and purified as previously described [66,67]. 2D ^{1}H-^{15}N HSQC (heteronuclear single-quantum coherence) experiments were acquired and analyzed as described [46,58]. Data were collected at 25 °C on a Bruker Avance DRX-500 spectrometer equipped with a triple-resonance probe and z-gradients. Samples contained NQO1 proteins (at 300 μM in monomer) and ^{15}N-labelled SAMp73α (300 μM) in 50 mM phosphate buffer at pH 6.9 with 200 μM of FAD.

2.13. Molecular dynamics (MD) simulations

Molecular dynamics of NQO1 in the dimeric form was performed by using the GROMACS package [68], largely following a protocol previously applied [53]. Eight simulation runs were carried out, differing by the absence or presence of (1) the FAD cofactor (apo- and holo-states, respectively), (2) the P187S polymorphism, and (3) the phosphomimetic mutation S82D. The protein structures were built starting from the crystallographic structure of the holo protein (PDB entry 1D4A [49]). Addition of a few missing atoms and residue modifications at the mutation sites were carried out *in silico* by using Visual Molecular Dynamics (VMD) [69].

The protein was solvated in a rhombic dodecahedron box with a minimum distance of 1 nm from each wall, resulting in ~17,800 water molecules, and Cl^- counterions were added to obtain an overall neutral system charge. Classical molecular dynamics was performed with periodic boundary conditions in the isothermal-isobaric ensemble, using the AMBER force field 99SB-ILDN for the protein [70], the generalized AMBER force field (GAFF) for FAD [71], and the TIP3P model for water [72]. Other conditions, including reference values and coupling times for the thermostat and barostat, modeling of non-bonded Coulomb and van der Waals interactions, and distance constraints on bonds, were as previously described [73,74]. Each simulation run was carried out with a sampling time of 1 ps for a total time of 100 ns.

The structural and dynamic properties of NQO1 were assessed by calculating atomic deviations and fluctuations in the protein structure, after rototranslation with a least squares fit to the C^{α} atoms with respect to the starting conformation to account for protein diffusion. Equilibration of protein inner motion was assessed by monitoring the root mean square deviations (RMSDs) of C^{α} atoms; 10 ns were typically sufficient for the holo-WT forms, and further analysis was carried out in the 20–100 ns time interval for ensuring a complete equilibration in all the cases. For all simulations, atomic deviation (RMSD) and fluctuation (root mean square fluctuation, RMSF) values were averaged on both protein monomers, and the two outmost residues at the N and C termini of the protein chains were excluded in the analysis due to their high mobility.

2.14. Expression analyses in eukaryotic cells

Site-directed mutagenesis to S82D or S82A was carried out on the pCINEO plasmids containing WT and P187S NQO1 sequences earlier described [58] and using the QuickChange lightening kit (Agilent Technologies, Madrid, Spain) following standard protocols. Mutagenesis was confirmed by DNA sequencing.

Caco-2 cells were grown, maintained, transfected and selected as described in [58]. Cells were lysed in RIPA buffer (50 mM Tris-HCl, 150 mM NaCl, 0.1% Triton X-100, 0.1% sodium dodecyl sulphate, 1 mM sodium orthovanadate, 1 mM NaF at pH 8) with protease inhibitors (COMPLETE, Roche, Spain). Upon centrifugation at 20000 *g* for 30 min at 4 °C, soluble protein extracts were collected and denatured with Laemmli's buffer under reducing conditions. Samples were resolved using 12% SDS-PAGE and transferred to polyvinylidene difluoride membranes (GE Healthcare) using standard procedures. Immunoblotting was carried out using primary monoclonal antibodies anti-NQO1 (sc-393,736, that recognizes the amino acids 249–270 at the C-terminus) and anti-β-actin from mouse at 1:500 and 1:10000 dilutions, respectively. As secondary antibody, chicken anti-mouse IgG-HRP were used at 1:2000 dilution. All antibodies were purchased from Santa Cruz Biotechnology. Samples were visualized using luminol-based enhanced chemiluminiscence (from BioRad Laboratories).

2.15. Activity measurements

NQO1 activity was measured in 50 mM K-HEPES at pH 7.4 and 25 °C. Experiments were carried out in a thermostatized Agilent 8453 diode-array spectrophotometer using 1 cm plastic cuvettes. For purified NQO1 proteins, the reaction contained NQO1 (1 nM for WT and S82D and 1–4 nM for P187S and P187S/S82D), 10 μM FAD and 0.5 mM NADH. This mixture was incubated for 5 min at 25 °C. The reaction was then triggered by the addition of 2,6-Dichlorophenolindophenol (DCPIP, final concentration of 50 μM) as the electron acceptor. Initial reaction rates were determined from time-dependent changes in A_{600nm} resulting from the reduction of DCPIP. Blanks without NQO1 were measured to account for the non-enzymatic reaction rates and subtracted. The activity was calculated using $\varepsilon_{600\ nm} = 21{,}000\ M^{-1}\cdot cm^{-1}$ for DCPIP and reaction rate constants (k) were determined by dividing the reaction rates by the NQO1 concentration.

For activity measurements in cell extracts, cells were grown as described in Section 2.14, collected in 50 mM K-HEPES at pH 7.4 with protease inhibitors (COMPLETE, Roche, Spain) and lysed by freezing-thawing cycles. Soluble extracts were those supernatants obtained upon centrifugation at 18000 *g* for 20 min at 4 °C. Total protein concentration was determined by the BCA method (Pierce) and extracts were immediately used for measurements. Activity measurements were carried out as describe above for purified proteins, and using 50–150 μg of total protein and 50 μM FAD. Upon blank subtraction, the activity was normalized by the amount of total protein used (50–150 μg) to obtain specific activities.

3. Results

3.1. Phosphorylation at S82 could modulate NQO1 stability linked to FAD binding affinity

As previously noted, NQO1 is a paradigm of flavoprotein in which intracellular degradation is coupled with the levels of the (flavin-free) apo-state [5]. In addition, the cancer-associated P187S variant decreases FAD binding affinity, and its ubiquitinylation and proteasomal degradation occurs efficiently either in the apo- or holo-states [5,53]. According to the PhosphoSite Plus® database, human NQO1 contains nine potentially active phosphorylation sites (S40 and S82, as well as Y20, Y43, Y68, Y76, Y127, Y129 and Y133), all of them located in the NTD [75]. Among them, we decided to investigate the consequences of phosphorylating S82 through a phosphomimetic S82D mutation, because: i) intracellular phosphorylation of S82 is well established and validated by 13 different HTPs, and well conserved across mammalian NQO1 (human, rat and mouse NQO1) although the kinase(s) responsible for its phosphorylation are not known; ii) mutations to E or D should mimic more realistically serine phosphorylation than tyrosine phosphorylation [76–79]; iii) a phosphomimetic strategy allows one to obtain site-specific and homogenous protein preparations for *in vitro* studies, while their use in transfected cells allows one to *switch on* (S82D) and *off* (S82A) the modification, thus providing a characterization of these two limiting behaviors (i.e. full vs. non phosphorylated, respectively); and iv) previous analyses by MALDI-TOF mass-spectrometry and peptide fingerprinting showed that NQO1 as recombinantly expressed in *E. coli* is not phosphorylated in this position [46,47]. This was confirmed by a side by side characterization of purified WT and P187S proteins carrying either S82A or S82D mutations (Fig. S3).

Structural and modeling studies on NQO1 predicted a significant effect of phosphorylating S82 on the stability and function of NQO1. The X-ray crystallographic structures showed that S82 was moderately solvent-exposed (20 ± 5% solvent exposure, from the structures with PDB codes 2F1O, 5FUQ and 4CF6) and it was located relatively far away from the FAD bound molecule (distance ≥ 15 Å) (Fig. 2A). However, S82 was located next to the loop 57–66, a region whose dynamics is affected by the P187S polymorphism that reduces FAD binding affinity [52,53,58]. The dynamics of this loop was previously shown to be linked with the evolutionary divergent electrostatic network involving E71, E78 and R/H80 [52,53,58]. These sequences adjacent to the phosphorylatable S82 are well-conserved across mammalian sequences and located mostly exposed to the solvent (Fig. 2B). Although the kinase (s) responsible for S82 phosphorylation are unknown so far, sequence analyses using pkaPS (http://mendel.imp.ac.at/pkaPS/) supported that S82 in the human sequence was a potential hit for PKA mediated phosphorylation (Fig. 2B). Interestingly, the R80H transition, that recently occurred during primate evolution facilitating NQO1 inactivation due to P187S [52,58], may have rendered this sequence less prone towards PKA phosphorylation (Fig. 2B). Modeling phosphorylation of the S82 or the phosphomimetic mutation S82D on the crystallographic structure of NQO1 (PDB code 2F1O; [63]) led to similar orientations of this amino acid side-chain and slightly increased its solvent exposure from 14% to 28% (Fig. 2A). Predicted changes in thermodynamic stability by FoldX determined using these models in the apo-state also supported that either phosphorylation or the phosphomimetic mutation S82D may locally increase the stability of apo-NQO1 by ~1.5 $kcal\cdot mol^{-1}$, partially overcoming the ~7 $kcal\cdot mol^{-1}$ destabilization caused by P187S.

3.2. Effect of the phosphomimetic mutation S82D on the conformation and stability of NQO1 in vitro

To experimentally characterize the effects of the phosphomimetic mutation S82D on NQO1 WT and the cancer-associated polymorphism P187S, four variants were recombinantly expressed, purified and

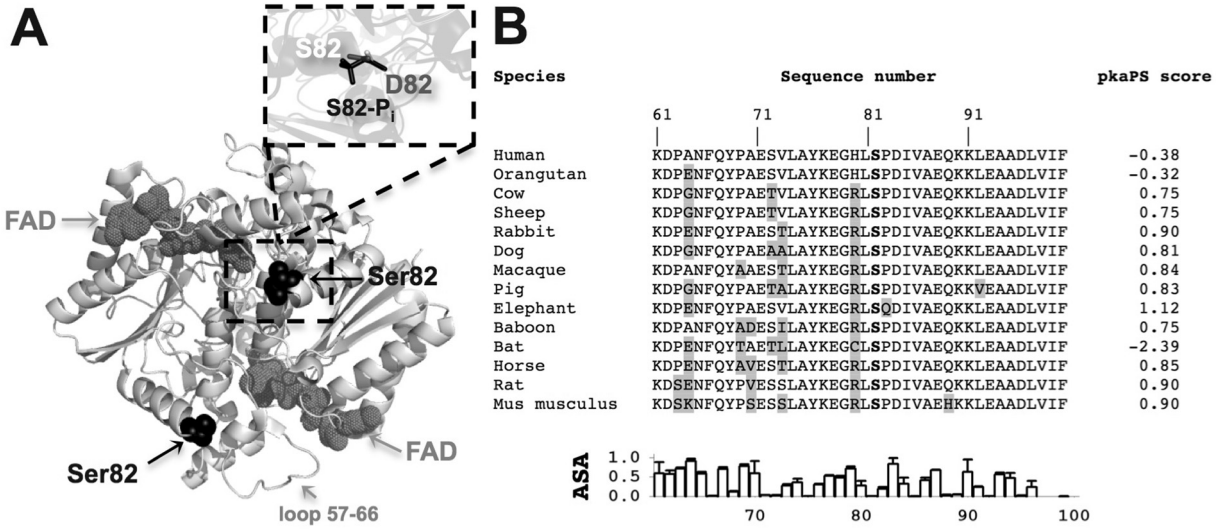

Fig. 2. Structural features of the phosphorylation site at S82 in NQO1. A) Location of S82 and the FAD binding pocket in the dimeric structure of NQO1. Inset: structural models for phosphorylated (S82-P_i) and phosphomimetic mutation (S82D) obtained using YASARA and the NQO1 structure (PDB code 2F1O). B) Conservation of the amino acid sequence adjacent to the phosphorylation site at S82. The phosphorylation score was determined using pkaPS [59] and the fractional (solvent) accessible surface area (ASA) was determined using GETAREA [62]. Data for ASA were mean ± s.d. from six NQO1 crystallographic monomers (from PDB codes 2F1O, 5FUQ and 4CF6).

characterized in detail: the WT protein, the single variants P187S and S82D, and the double mutant P187S/S82D. All the variants were highly active, although the activity of P187S and P187S/S82D was slightly lower (Fig. S2). The phosphomimetic mutation had no noticeable effect on the secondary structure or the hydrodynamic volume of the folded dimer as apo-protein (Fig. S4). Reconstitution of holo-enzymes led to an increase in secondary structure and a more compact dimeric conformation (Fig. S4) in WT, but these effects were smaller in P187S, possibly

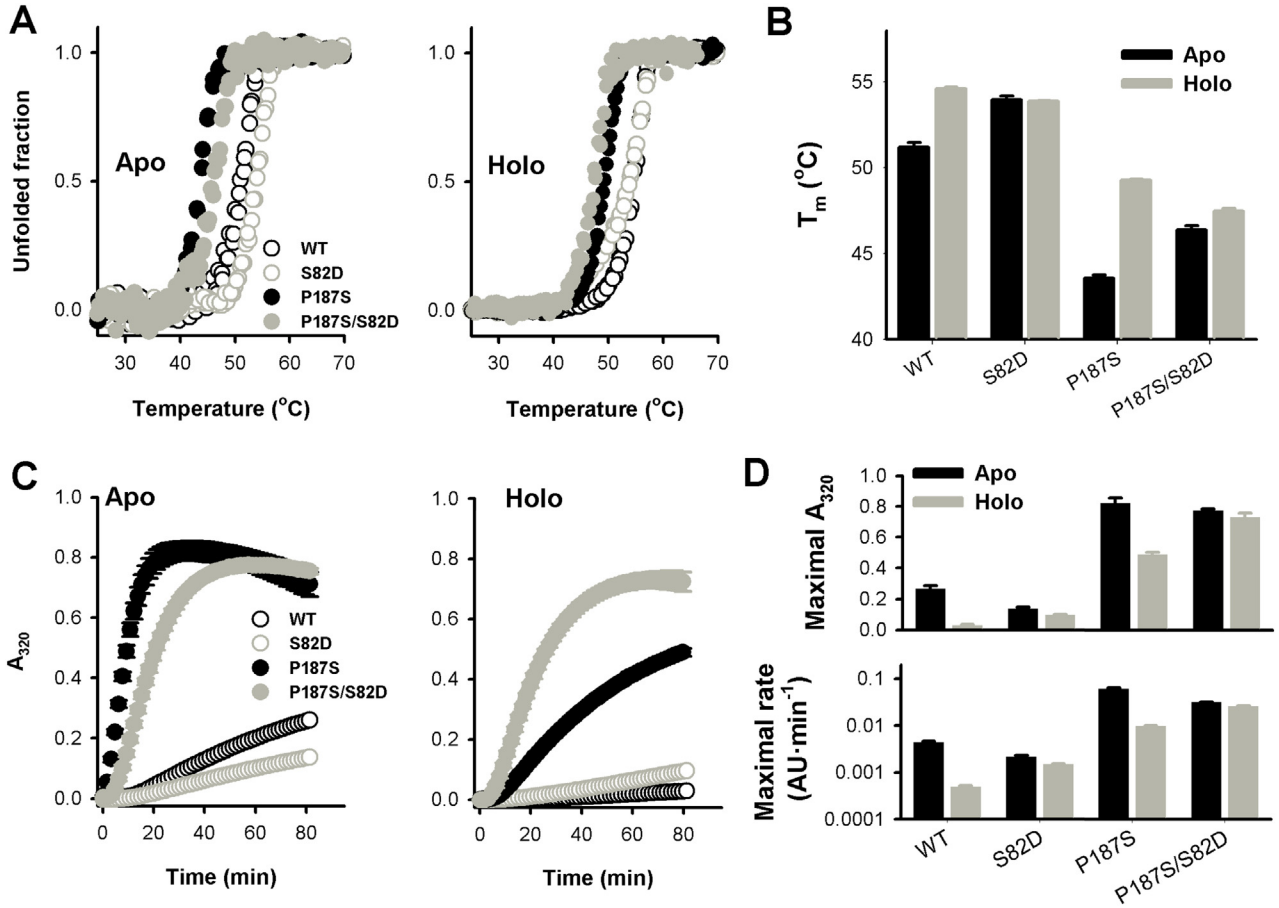

Fig. 3. Effect of the phosphomimetic mutation S82D on the conformational stability and aggregation of apo- and holo-NQO1. A–B) Thermal denaturation profiles of WT and P187S variants (A) and their corresponding T_m values (B). C) Aggregation kinetics monitored by turbidity measurements (A_{320}) at 37 °C; D) Maximal turbidity values (upper panel) and aggregation rates (lower panel). Data in A and C were from three independent measurements, and in B and D, the mean ± s.d. ($N = 3$) were reported. Experiments were performed using 2 μM apo-proteins in the absence or presence of an excess of FAD (20 μM).

due to its partially unfolded CTD in the holo-state (in agreement with previous reports; [5,46,47,53]). The conformation of WT and P187S in the apo- or holo-states was not affected by the mutation S82D (Fig. S4).

We then evaluated the consequences of the mutation S82D on the conformational stability by thermal denaturation experiments (Fig. 3A). The phosphomimetic mutation stabilized both WT and P187S in the apo-state, but abolished the stabilization exerted by FAD binding (Fig. 3A–B). Whereas the overall conformational stability of NQO1 variants poorly correlated with their intracellular turnover [5,46,53], its aggregation propensity has been associated with coaggregation of other proteins such as the amyloid β-peptide [5]. We thus measured NQO1 aggregation kinetics in both the apo- and holo-states at physiological temperature (Fig. 3C–D). The results obtained followed the same trend observed for the effects of P187S and S82D on thermal stability. As apo-proteins, the maximal aggregation rate for P187S was about 15-fold faster than that of WT, whereas the S82D mutation slowed down aggregation by 2- to 3-fold in either WT or P187S (Fig. 3C–D). Binding of FAD slowed down the aggregation of WT and P187S by 9- and 6-fold, respectively, whereas FAD binding hardly affected aggregation of WT or P187S containing the phosphomimetic mutation (Fig. 3C–D). Therefore, phosphorylation of WT and P187S NQO1 may increase their tendency to aggregate under normal or high riboflavin intracellular contents (in which cases the holo-state is expected to be highly populated [80]), with a potential impact on the aggregation of other disease-associated proteins such as the amyloid β-peptide [5].

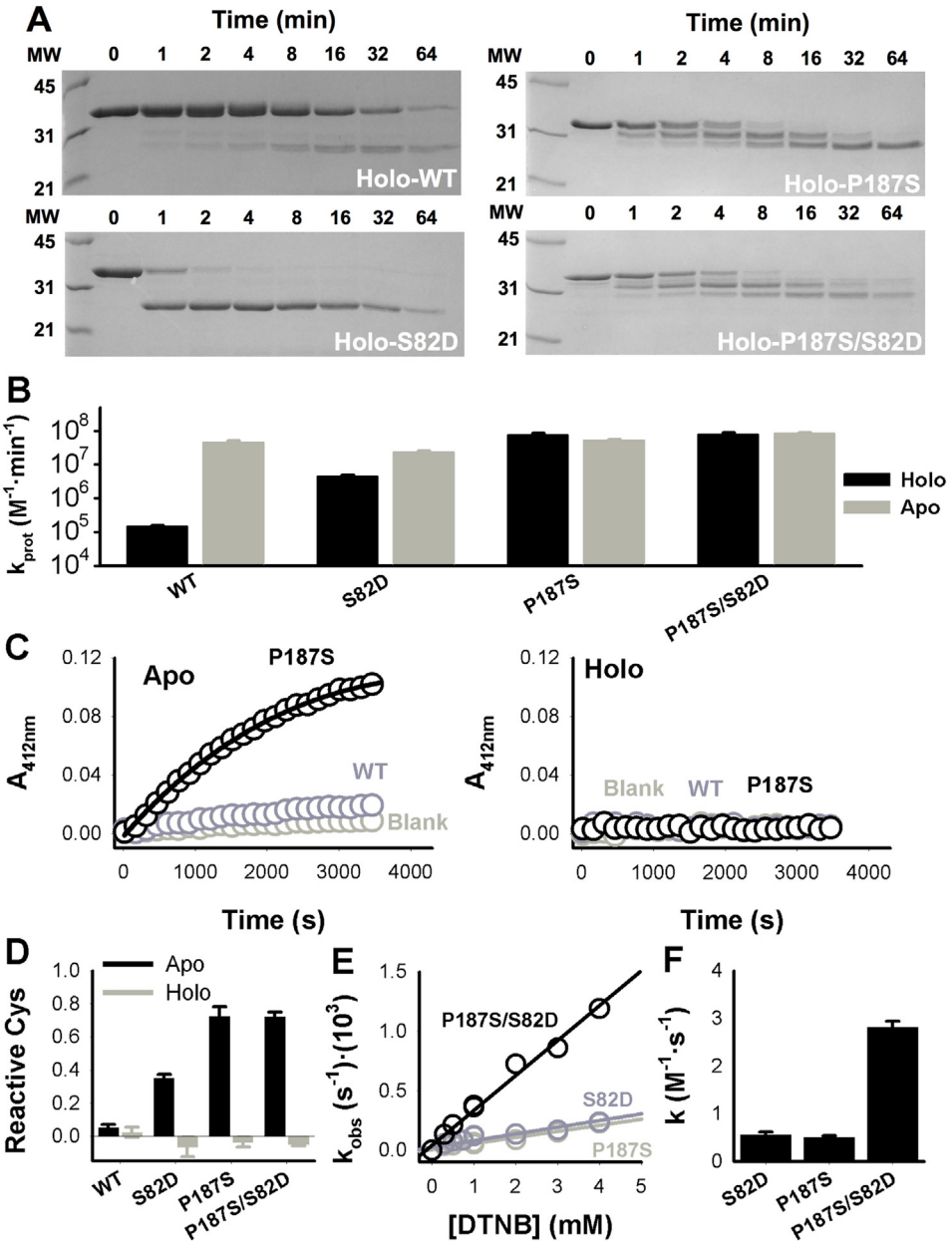

Fig. 4. Effect of the phosphomimetic mutation S82D on protein local stability and dynamics from proteolysis and thiol-modification kinetics. A) Representative SDS-PAGE analyses of proteolysis kinetics for holo-NQO1 proteins with thermolysin (200 nM in WT and S82D, and 5 nM protease in P187S and P187S/S82D enzymes, respectively). B) Proteolysis second-order rate constants (k_{prot}) for holo- and apo-NQO1 proteins, determined from three independent measurements of each variant; C) Reaction kinetics of 1 mM DTNB without (blank) or with 10 μM NQO1 proteins (apo- and holo-proteins); D) Fraction of C180 titrated by DTNB per NQO1 monomer quantified using the A_{412} after 1 h of reaction (mean ± s.d. from at least three independent experiments). E–F) Dependence of pseudo first-order rate constants on DTNB concentration (E) and corresponding second-order rate constants (F, slopes ± S.E. from linear fittings in panel E).

3.3. The phosphomimetic mutation S82D perturbs the dynamics of the NTD and decreases the affinity for FAD

The consequences of P187S on NQO1 intracellular stability and function are fundamentally linked to changes in protein local dynamics at the CTD and NTD, respectively [53,58]. These changes can be experimentally and quantitatively assessed using partial proteolysis kinetics [53,58,65]. We thus performed proteolysis experiments in the NQO1 variants WT, S82D, P187S and P187S/S82D (Figs. 4 and S5). The proteolysis patterns of either WT or P187S NQO1 were not changed by the S82D mutation: holo-WT was cleaved at the N-terminus (between residues 72–73 [53]) leading to the accumulation of a 22.8 kDa fragment, whereas holo-P187S and all apo-NQO1 variants were cleaved at the CTD (between residues 235 and 237 [53]) leading to the accumulation of 29.9 and 28.2 kDa fragments (Figs. 4A and S5). Remarkably, the presence of S82D accelerated proteolysis of holo-WT by 30-fold, revealing increased dynamics of the NTD (Fig. 4A–B). The local effects on the NTD due to S82D did not propagate to the CTD, as shown by the small effects of the phosphomimetic mutation on the apo-NQO1 and holo-P187S proteins (Figs. 4B and S5). According to recent works [46,52,53,58], these alterations caused by S82D in the local stability/dynamics around the FAD binding site could affect binding of the flavin to NQO1.

To detect further effects of the phosphomimetic mutation on protein local stability and dynamics that might not be revealed by proteolysis experiments, we carried out kinetic experiments of thiol-modification with DTNB. NQO1 contains a single cysteine (C180) which is fully buried in the X-ray crystal structures (the solvent accessible surface area was null in the structures with PDB codes 2F1O, 4CF6 and 5FUQ). In these structures (obtained with both FAD and dicoumarol bound), C180 was distant to the FAD binding site (shortest distance ≥ 10 Å), S82 or P187 (≥15 Å) or the N-terminal and C-terminal cleavage sites for thermolysin (≥10 Å). However, due to the highly dynamic nature of NQO1 [35,46,47,53,58], it is possible that C180 is (at least transiently) solvent-exposed in the apo-state due to conformational fluctuations. Indeed, C180 in apo-P187S reacted to a large extent with DTNB, while its reactivity with apo-WT was negligible (Fig. 4C–D). Interestingly, the phosphomimetic mutation did not affect the fraction of C180 titrated with DTNB in apo-P187S, but increased notably this fraction in apo-WT (Fig. 4C–D). Importantly, the reactivity of C180 with DTNB observed in apo-NQO1 containing P187S and/or S82D was fully abolished when these variants bound FAD (Fig. 4C–D). It is plausible that the high reactivity of C180 towards DTNB observed in those variants containing P187S and/or S82D is due to enhanced conformational fluctuations in the apo-state. To confirm this hypothesis, we determined the rate constants for this reaction (Fig. 4E). We found for this constant a value of $0.50 \pm 0.03\ M^{-1}\ s^{-1}$ in apo-P187S (Fig. 4F), which is 5000-fold lower than that obtained for free L-Cys ($2.44 \pm 0.15 \cdot 10^{3}\ M^{-1}\ s^{-1}$). This low, but not null, value for this rate constant suggested that C180 in the apo-state of P187S was only transiently exposed and available for the reaction with DTNB. Interestingly, apo-S82D showed virtually the same value for the rate constant than that of apo-P187S, while modification of C180 in apo-P187S/S82D was 6-fold faster than those of the single mutants (Fig. 4E and F). Additional support for this interpretation of DTNB reaction kinetics came from its small dependence on denaturant concentration, consistent with a local structural fluctuation coupled to the reaction of C180 with DTNB (Fig. S6).

To test whether the dynamic alterations induced by the phosphomimetic mutation in the NTD affected FAD binding, we determined FAD contents in NQO1 variants as they are purified as well as the binding equilibrium constants for FAD using apo-proteins. The FAD content of NQO1 proteins from IMAC purification showed a significant decrease for both WT and P187S in the presence of S82D (Fig. 5A and B). According to previous studies [51,53,58], these lower contents

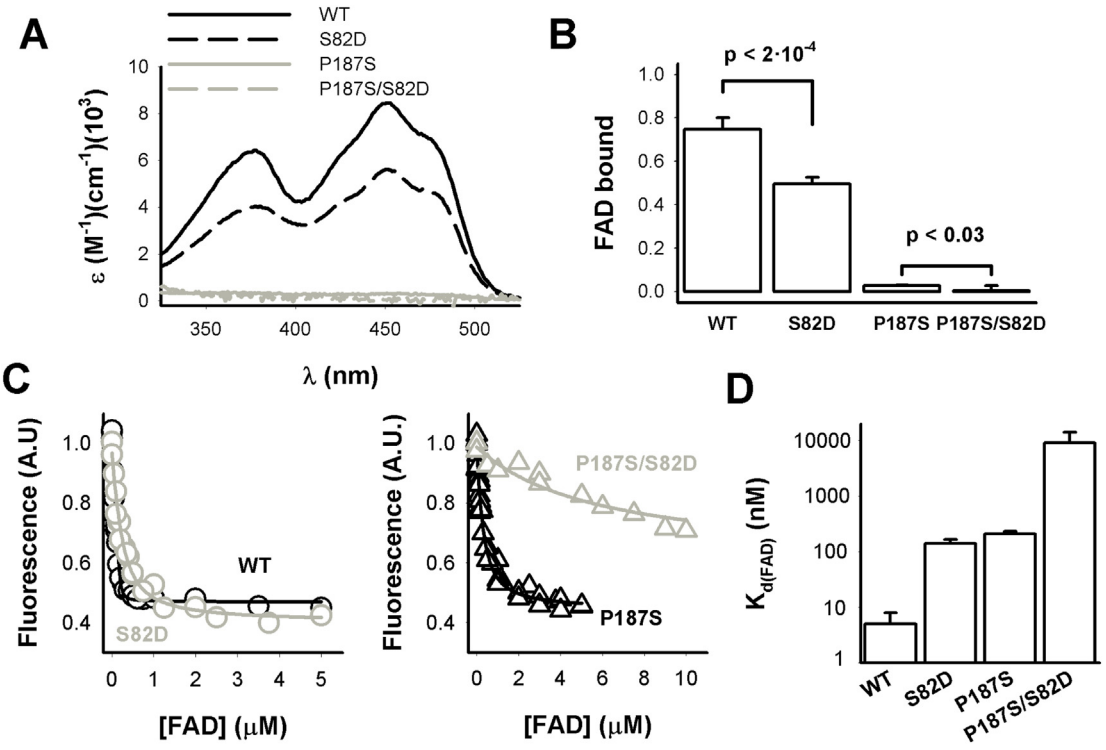

Fig. 5. Effect of the phosphomimetic mutation S82D on FAD binding. A) Near UV–visible absorption spectra of NQO1 proteins as purified (average from four independent purifications). B) Fraction of NQO1 monomer with FAD bound as they are purified. Data were means ± s.d. from four independent purifications. Statistical significance was obtained from a two-tailed unpaired *t*-test; C) Fluorescence titrations of apo-NQO1 proteins with FAD. Lines were best-fits to a 1:1 interaction model; D) K_d values for the FAD:NQO1 interaction. Values were those derived from fittings shown in panel C (with the corresponding fitting errors). Titrations for WT and P187S in panel C and the estimated $K_{d(FAD)}$ values in panel D were from [58] and reproduced with permission.

in FAD due to the S82D mutation would indicate lower binding affinities. Direct titrations of apo-proteins with FAD showed that the mutation S82D decreased binding affinities by about 20-fold in both WT and P187S (Fig. 5C–D and S7). Noteworthy, the variant P187S/S82D showed almost 1000-fold lower affinity for FAD than WT NQO1. These results suggested that phosphorylation of S82 may substantially shift the FAD binding equilibrium towards the apo-state under physiological conditions, particularly in combination with P187S.

3.4. The phosphomimetic S82D mutation affects but does not abolish the interaction of NQO1 with SAMp73α

One of the most important functions of NQO1 is its ability to interact with a variety of protein partners (such as p53 or p73α) leading to their stabilization intracellularly [36,38,81,82]. One of the most studied and important protein partners of NQO1 is the tumour suppressor p73α [46,82]. The presence of an active NQO1 seemed to play a role in the interaction with the C-terminal SAM domain of p73α (named here as SAMp73α) [82], although NQO1 forms with low activity such as the polymorphic P187S (essentially an apo-protein), the WT protein bound to the inhibitors dicoumarol or ES936, or the C-terminal truncated WT protein retained some capacity to bind p73α [46,83].

To prove the effects of S82D in these protein:protein interactions mediated by NQO1, we acquired 2D HSQC NMR spectra of ^{15}N-SAMp73α in the presence of WT, S82D, P187S and P187S/S82D proteins. The interaction with NQO1 proteins caused changes in chemical shifts or, alternatively, signal broadening in the HSQC spectra of SAMp73α (Fig. S8 showed some representative examples). Although the phosphomimetic mutation did not abolish the interaction with SAMp73α, the set of residues whose signals were affected upon binding was smaller in those variants containing S82D, particularly for the α-helices 3 and 4 and the helix 3_{10} (Fig. 6). Overall, these results suggested that phosphorylation of S82 may affect the affinity and/or the binding mode for the interaction between NQO1 and SAMp73α.

3.5. Local structural and dynamics alterations due to the phosphomimetic mutation S82D are probed by MD simulations

Previous MD simulations have indicated that inactivation and destabilization of NQO1 by P187S and its rescue by the H80R mutation have structural and dynamic basis [46,52,53,58]. In this section, we show that the impact of phosphomimetic S82D on the affinity for FAD and its opposite effects on the conformational stability of holo- and apo-NQO1 are associated with changes in local structure and dynamics, further supporting our interpretation of experimental analyses from proteolysis and DTNB reaction kinetics

Our MD simulations did not reveal large changes in either the overall structure or the FAD binding site by the S82D mutation (Fig. S9). However, we noted some local changes in the conformation of residues 50–70 only in the apo-state, which occurred in the surroundings of the FAD binding site (Fig. 7A–C). This region, particularly the loop 58–67 and the cluster of electrostatic interactions between E71, E78 and H/R80 are important to modulate FAD binding affinity [52,53]. In agreement with previous studies [53], this region also manifested a large decrease in backbone dynamics upon FAD binding (Figs. 7D and S10). Interestingly, the presence of S82D seemed to reduce this change in dynamics upon FAD binding by decreasing the fluctuations of this region in the apo-state and increasing them in the holo-state (Figs. 7D and S10). Mapping of these dynamic alterations onto the structure of NQO1 also showed that the effects of S82D propagated through the neighbouring FAD binding site, affecting only small sets of residues in the CTD (Fig. 7E). These changes in dynamics and structure due to the

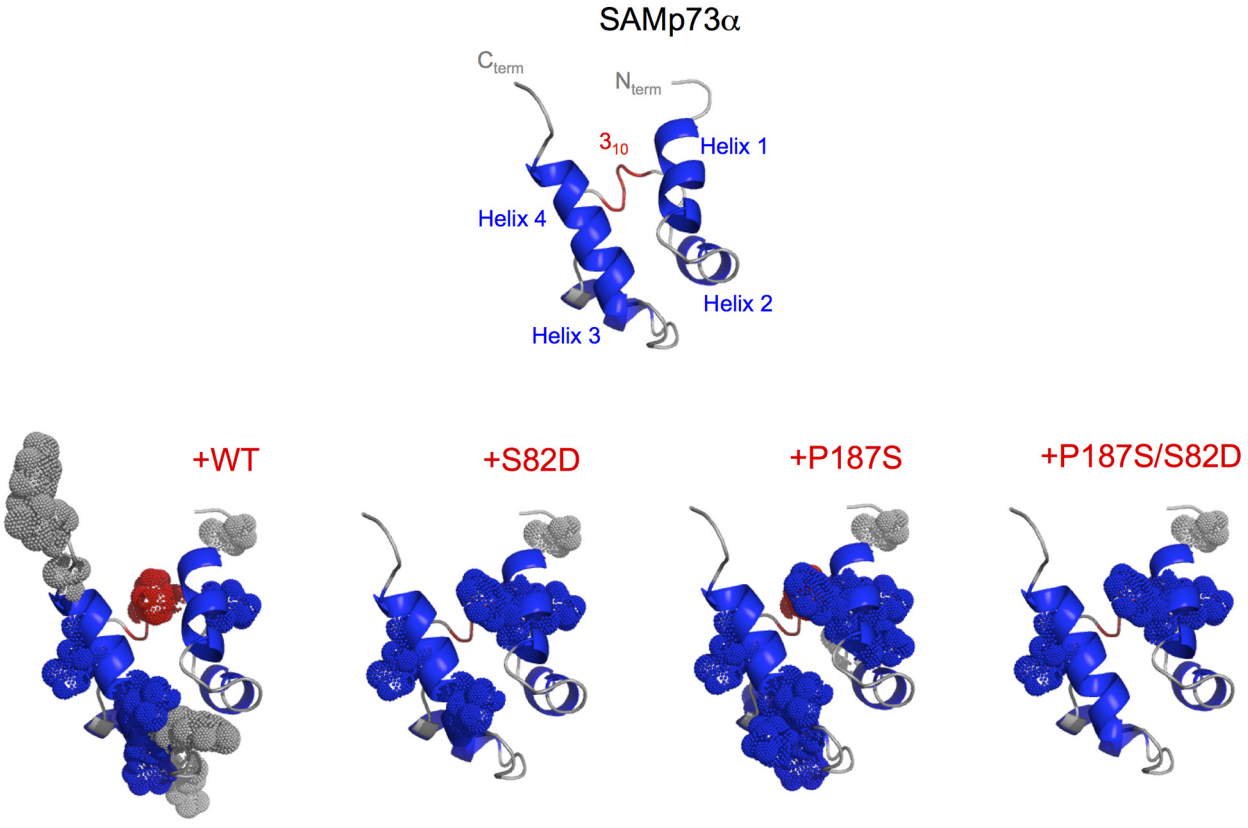

Fig. 6. The effect of the phosphomimetic mutation S82D in the interaction of NQO1 with SAMp73α measured by 2D ^{1}H-^{15}N HSQC NMR spectroscopy. Structure of SAMp73α (PDB entry 1COK) highlighting different secondary structure ordered elements and those residues affected in the presence of NQO1 variants (as spheres).

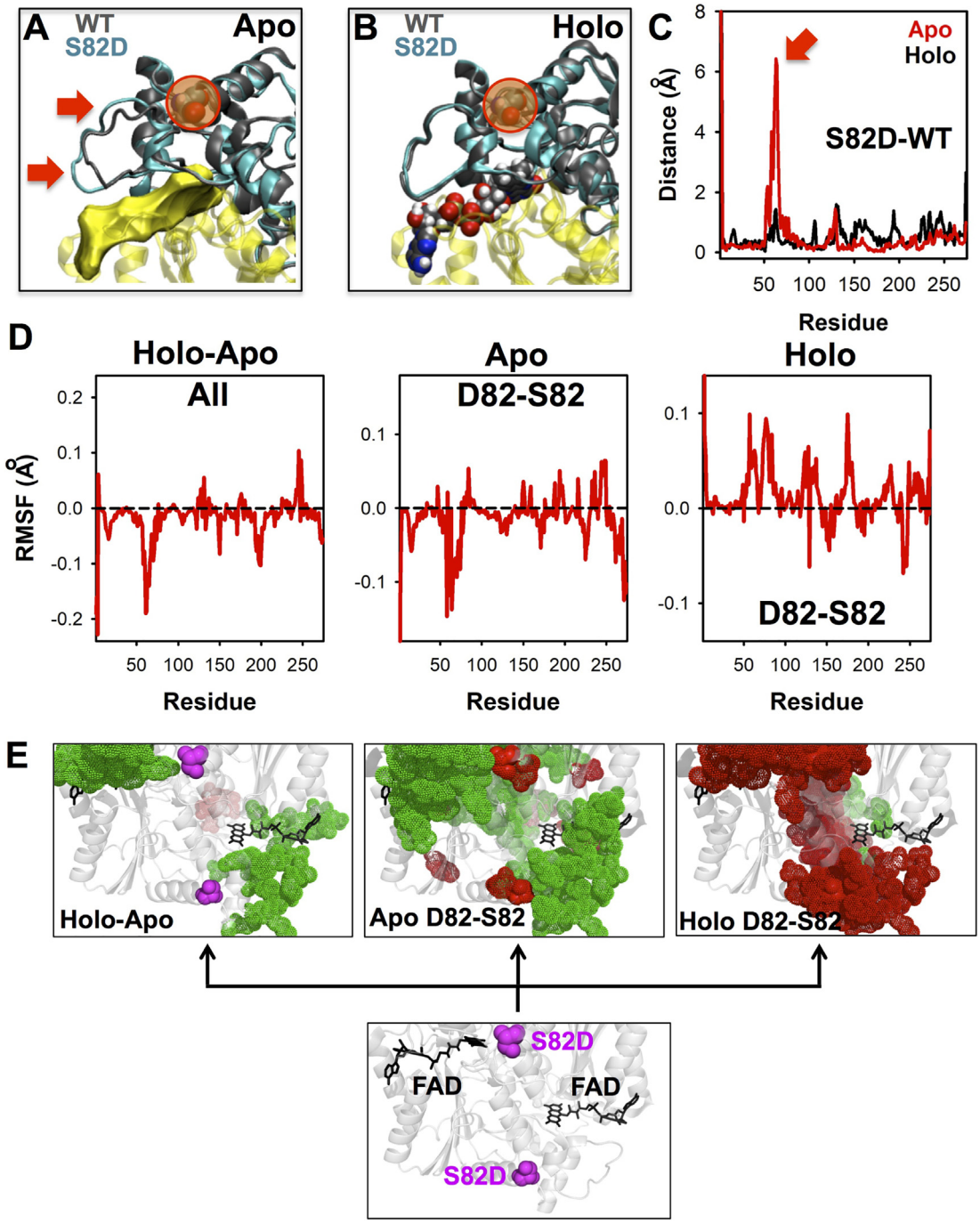

Fig. 7. Structural and dynamic changes in the FAD binding site due to the mutation S82D from MD simulations. A–C) Structural overlay of the effect of S82D on the averaged MD structures of apo- and holo-species (A–B, in grey and cyan). The FAD molecule was shown in surf (apo) and van der Waals representation (holo). The S82/D82 residue was highlighted with a red circle. Residues 50–70, showing the largest structural differences in the apo state, were highlighted with red arrows in panel A and C). D) Comparison of backbone dynamics (RMSF) between protein species: difference between all holo-states vs. all apo-states (left), and between variants containing D82 and S82 in the apo-(middle) and holo-states (right). E) Structural location of residues with larger effects on the dynamics (RMSF variation > 0.05 Å, right panel, and >0.02 Å, middle/left panels) corresponding to the data shown in panel D. Residues in green/red displayed decreased/increased dynamics (i.e. negative/positive values in the plots of panel D), respectively.

S82D mutation revealed by MD simulations contributed to explain at the molecular level the remarkable decrease in FAD binding affinity that phosphorylation may cause.

3.6. The phosphomimetic mutation strongly decreased WT protein levels in cells

To test the consequences of phosphorylation at S82 on the steady-state levels of NQO1, we carried out expression analyses on stably transfected Caco-2 cells using procedures recently described [58]. Introduction of the phosphomimetic mutation led to a 3-fold decrease in WT NQO1 protein levels and a concomitantly lower activity, whereas the effects of S82D on P187S were small (Fig. 8). Due to the well-established relationship between the intracellular protein levels of WT NQO1, its rate of proteasomal degradation and the population of the apo-state [5,35], these results suggested that the phosphomimetic mutation increased the degradation rate of WT NQO1 intracellularly by promoting the formation of the degradation-prone apo-state.

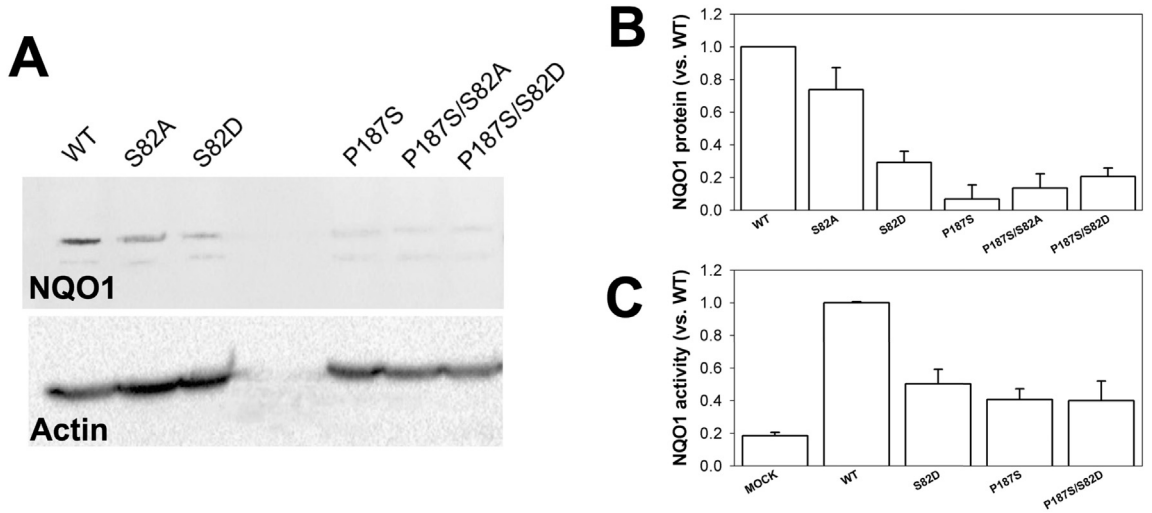

Fig. 8. Effects of the phosphomimetic mutation S82D on the expression levels of NQO1 in stably transfected Caco-2 cells. A) Western-blot analyses in soluble extracts using anti-NQO1 and anti-β-actin primary antibodies. B) Expression levels obtained from three different experiments and normalized vs. those of WT NQO1. Data were reported as mean ± s.d. from three independent measurements. C) NQO1 activity in soluble cell extracts and normalized vs. those of WT NQO1 (63.2 ± 0.4 nM DCPIP·min^{-1}·μg^{-1} protein). Specific activities were determined from the linear slope of activity vs. protein concentration plots from at least four independent measurements. The label "mock" in panel C refers to the activity of stably transfected Caco-2 cells with the empty (no NQO1 cDNA) pCINEO plasmid, and thus provide the background NQO1 activity in these cells.

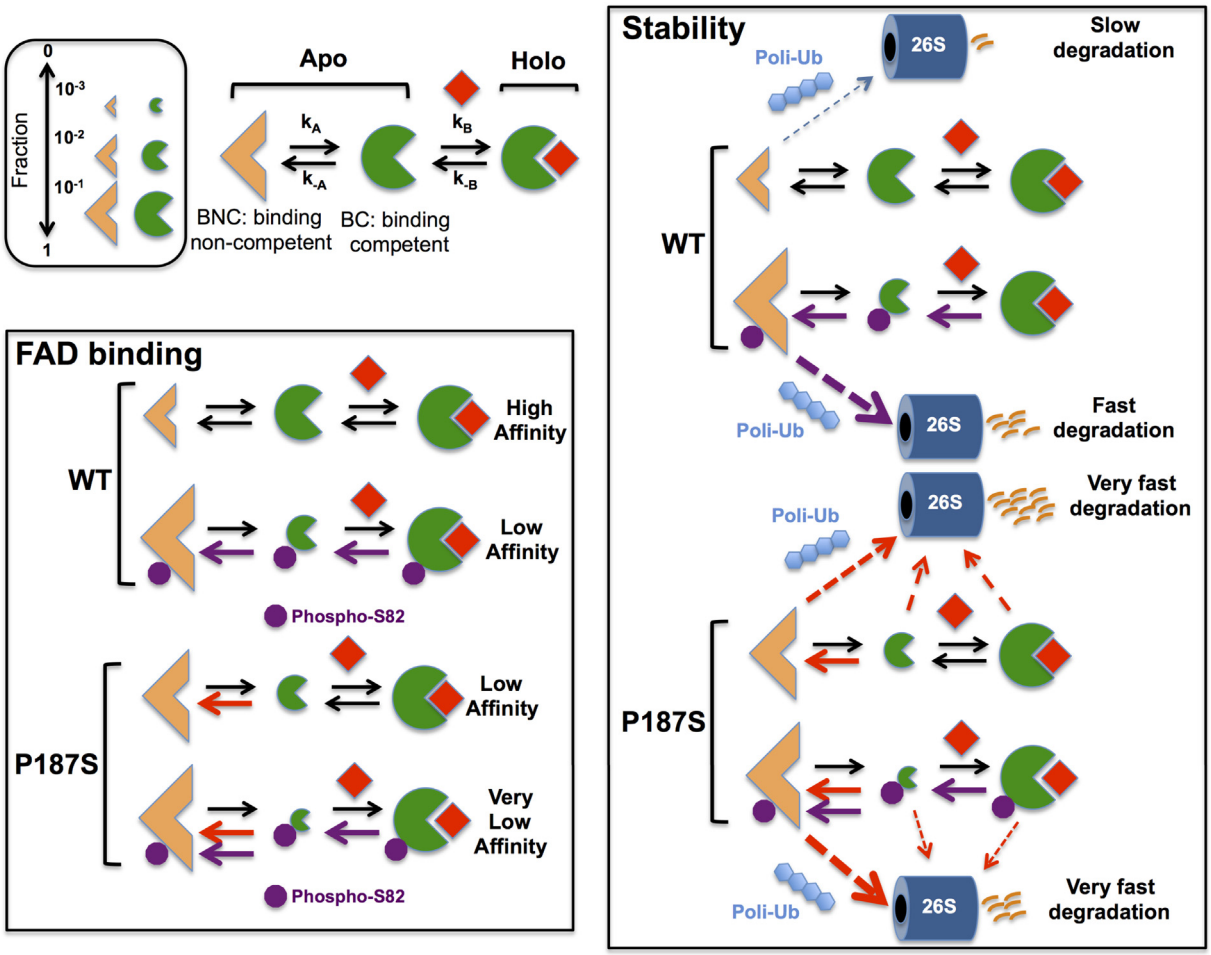

Fig. 9. Molecular mechanisms describing the proposed link between the effects of S82D on FAD binding and the intracellular stabilities of WT and P187S NQO1. In the absence of FAD, the conformational equilibrium of the apo-state contains binding non-competent (BNC) and binding competent (BC) substates according to previous analyses (see [52]). The size of the symbols corresponding to BNC and BC substates roughly reflects the population of these states.

4. Discussion

Comprehensive analysis of protein phosphorylation, as well as other PTMs, through large-scale proteomic approaches has revealed remarkable complexity and subtleties, with potentially profound implications to understand cellular metabolism as well as its dysfunction in disease [3,84–88]. One of the challenges ahead is characterizing the effects of such PTMs on biological function and activity. Regarding the flavoproteome, a set of about 100 human proteins involved in multiple cellular and metabolic roles and inherited diseases [4], only a small fraction of identified protein phosphorylation events in a few flavoprotein targets have been investigated so far (Fig. 1). Particularly important, the effects of phosphorylation on flavin binding and flavoprotein stability have not been previously addressed, to the best of our knowledge. To provide insight into this issue, we carried out a thorough analysis of the molecular consequences caused by the phosphomimetic mutation S82D on the stability and flavin binding of human NQO1. NQO1 is one of the best examples of a flavoprotein with a strong *in vivo* dependence between flavin binding and protein stability, which is also perturbed by the cancer associated P187S polymorphism [5,35,40,47,51,53,58]. Our results revealed that phosphorylation at S82 may affect the structure and dynamics of regions next to the FAD binding site, strongly decreasing protein levels (and stability) of WT NQO1 under normal riboflavin availability.

The results gathered in this work, together with previous results [5,35,46,47,52,53,55,58], allow us to propose mechanisms linking the molecular consequences of mimicking phosphorylation of NQO1 at S82 (investigated through the phosphomimetic mutation S82D) with their effects in protein structure, dynamics and FAD binding (Fig. 9). These mechanisms also suggest a molecular framework that provides a reasonable explanation for the different intracellular response of WT and P187S to the phosphomimetic mutation. According to general models of allostery [89], WT NQO1 exists in the apo-state in equilibrium between two conformational substates or populations, one corresponding to FAD binding non-competent (BNC) substates (resembling the expanded and highly dynamic state observed by experiments and simulations) and the other to FAD binding competent (BC) substates (i.e. those resembling the structure of the protein in the holo-state but without FAD bound) [52]. Previous analyses have indicated that the BNC substates are highly populated in the absence of FAD [52]. Addition of FAD leads to a shift between the populations of BNC towards BC substates due to the preferential binding of FAD to the latter [52,89]. Our MD simulations supported that S82D locked the conformation of the FAD binding site; this shifted the conformational equilibrium in the apo-protein towards the BNC substates, which in principle should reduce the overall FAD association rates. In addition, the phosphomimetic mutation perturbed the dynamics of the FAD binding site in the holo-state, which may favor release of the cofactor thus speeding up the FAD dissociation rates (Fig. 9). These two effects may contribute to explain the large decrease in FAD binding due to the mutation S82D. In this context, the effects of the phosphomimetic mutation on FAD binding may be linked with those on protein stability inside cells. The effect of the S82D mutation may promote the population of the apo-state *in cellulo* by stabilizing the BNC substates. Concomitantly, such an increased population of the apo-state due to phosphorylation may speed up the ubiquitin-dependent proteasomal degradation of the WT protein, for which the population of apo-NQO1 is likely the rate-limiting factor (Fig. 9). Importantly, these consequences seemed somewhat different for P187S. The polymorphism may also undergo a similar shift in the conformational equilibrium towards the BNC substates, but possibly with small effects on the BC substates or the holo-state due to their inherent low population in P187S [52]. However, in the case of P187S, the effects of S82D had small consequences in the intracellular stability (Fig. 8), since either BNC, BC or the holo-state are targeted for proteasomal degradation due to the efficient ubiquitinylation of its flexible and partially unfolded CTD in both apo- and holo-states (Fig. 9 [5,53]). All these features could make P187S very susceptible to intracellular degradation whether or not S82 is phosphorylated (Fig. 9).

Overall, our work provided insight into the regulation of the stability of NQO1 with potential implications to understand its dual role in cancer development and treatment. The lack of NQO1 protein and activity of P187S is associated with increased cancer risk [40,43], leading to destabilization of oncosuppressors such as p53 and p73α [46,81,82] and preventing activation of cancer chemotherapies [56,64]. By contrast, the WT protein is overexpressed in certain types of tumours and its pharmacological inhibition is a promising approach to treat cancer through increased generation of reactive oxygen species [90–93]. In this context, an alternative approach to target cancer-associated NQO1 overexpression and activity of the WT protein could be the activation of kinase(s) or inhibition of phosphatase(s) controlling the phosphorylation at S82; this would lead to a concomitant decrease in NQO1 stability and protein levels. Obviously, this would require the identification of those kinases/phosphatases involved in this phosphorylation event.

Our results supported that phosphorylation, as well as ubiquitinylation [5], can be critical for the regulation of the activity and stability of NQO1, and more generally of many human flavoproteins given the general link between their flavin content and degradation rates inside the cell [5]. Importantly, the cross-talk between different PTMs (e.g. phosphorylation and ubiquitinylation) may add additional layers of regulation for the function and stability of human flavoproteins. In particular, our work underscores the importance of understanding how the effects of disease-associated mutations and PTMs can locally affect structural and dynamical properties and propagate through the structure to distant sites [46,53,58]. More generally, we also propose that understanding the effects of PTMs could provide a deeper understanding of genotype-phenotype relationships in loss-of-function genetic diseases.

Acknowledgments

We thank Prof. Francisco Conejero Lara (Department of Physical Chemistry, University of Granada) for the access to the DLS instrument. This work was supported by the Spanish Ministry of Economy and Competitiveness grant number CTQ2015-64445-R to J.L.N. and by Junta de Andalucia grant number P11-CTS-07187. E.M.C. was recipient of a predoctoral fellowship from Junta de Andalucia. R.M-E. is grateful for a FPU Grant (FPU14/01537) from the Ministry of Education of Spain. J.L.N. thanks C. Arrowsmith for the kind gift of the SAMp73α vector. B.R. acknowledges kind hospitality and the use of computational resources in the Magnetic Resonance Center (CERM), Sesto Fiorentino (Florence), Italy.

Appendix A. Supplementary data

Supplementary data to this article can be found online at https://doi.org/10.1016/j.ijbiomac.2018.09.108.

References

[1] A.F.M. Altelaar, J. Munoz, A.J.R. Heck, Next-generation proteomics: towards and integrative view of proteome dynamics, Nat. Rev. Genet. 14 (2013) 35–48.
[2] P.V. Hornbeck, B. Zhang, B. Murray, J.M. Kornhauser, V. Latham, E. Skrzypek, PhosphoSitePlus, 2014: mutations, PTMs and recalibrations, Nucleic Acids Res. 43 (Database issue) (2015) D512–D520.
[3] C.D. Terfve, E.H. Wilkes, P. Casado, P.R. Cutillas, J. Saez-Rodriguez, Large-scale models of signal propagation in human cells derived from discovery phosphoproteomic data, Nat. Commun. 6 (2015) 8033.
[4] W.D. Lienhart, V. Gudipati, P. Macheroux, The human flavoproteome, Arch. Biochem. Biophys. 535 (2) (2013) 150–162.
[5] A. Martinez-Limon, M. Alriquet, W.H. Lang, G. Calloni, I. Wittig, R.M. Vabulas, Recognition of enzymes lacking bound cofactor by protein quality control, Proc. Natl. Acad. Sci. U. S. A. 113 (43) (2016) 12156–12161.
[6] T.A. Giancaspero, M. Colella, C. Brizio, G. Difonzo, G.M. Fiorino, P. Leone, R. Brandsch, F. Bonomi, S. Iametti, M. Barile, Remaining challenges in cellular flavin cofactor homeostasis and flavoprotein biogenesis, Front. Chem. 3 (2015) 30.

[7] E.M. Torchetti, F. Bonomi, M. Galluccio, E. Gianazza, T.A. Giancaspero, S. Iametti, C. Indiveri, M. Barile, Human FAD synthase (isoform 2): a component of the machinery that delivers FAD to apo-flavoproteins, FEBS J. 278 (22) (2011) 4434–4449.

[8] B.S. Kim, L. Serebreni, J. Fallica, O. Hamdan, L. Wang, L. Johnston, T. Kolb, M. Damarla, R. Damico, P.M. Hassoun, Cyclin-dependent kinase five mediates activation of lung xanthine oxidoreductase in response to hypoxia, PLoS One 10 (4) (2015), e0124189.

[9] W. Luu, E.J. Zerenturk, I. Kristiana, M.P. Bucknall, L.J. Sharpe, A.J. Brown, Signaling regulates activity of DHCR24, the final enzyme in cholesterol synthesis, J. Lipid Res. 55 (3) (2014) 410–420.

[10] M. Ogura, J. Yamaki, M.K. Homma, Y. Homma, Mitochondrial c-Src regulates cell survival through phosphorylation of respiratory chain components, Biochem. J. 447 (2) (2012) 281–289.

[11] Y. Kabuyama, T. Suzuki, N. Nakazawa, J. Yamaki, M.K. Homma, Y. Homma, Dysregulation of very long chain acyl-CoA dehydrogenase coupled with lipid peroxidation, Am. J. Phys. Cell Phys. 298 (1) (2010) C107–C113.

[12] K. Yamada, J.R. Strahler, P.C. Andrews, R.G. Matthews, Regulation of human methylenetetrahydrofolate reductase by phosphorylation, Proc. Natl. Acad. Sci. U. S. A. 102 (30) (2005) 10454–10459.

[13] S. Adak, J. Santolini, S. Tikunova, Q. Wang, J.D. Johnson, D.J. Stuehr, Neuronal nitric-oxide synthase mutant (Ser-1412 –> Asp) demonstrates surprising connections between heme reduction, NO complex formation, and catalysis, J. Biol. Chem. 276 (2) (2001) 1244–1252.

[14] Y. Hayashi, M. Nishio, Y. Naito, H. Yokokura, Y. Nimura, H. Hidaka, Y. Watanabe, Regulation of neuronal nitric-oxide synthase by calmodulin kinases, J. Biol. Chem. 274 (29) (1999) 20597–20602.

[15] A. Tyryshkin, F.M. Gorgun, E. Abdel Fattah, T. Mazumdar, L. Pandit, S. Zeng, N.T. Eissa, Src kinase-mediated phosphorylation stabilizes inducible nitric-oxide synthase in normal cells and cancer cells, J. Biol. Chem. 285 (1) (2010) 784–792.

[16] D. Fulton, J.E. Church, L. Ruan, C. Li, S.G. Sood, B.E. Kemp, I.G. Jennings, R.C. Venema, Src kinase activates endothelial nitric-oxide synthase by phosphorylating Tyr-83, J. Biol. Chem. 280 (43) (2005) 35943–35952.

[17] D. Fulton, J.P. Gratton, T.J. McCabe, J. Fontana, Y. Fujio, K. Walsh, T.F. Franke, A. Papapetropoulos, W.C. Sessa, Regulation of endothelium-derived nitric oxide production by the protein kinase Akt, Nature 399 (6736) (1999) 597–601.

[18] M.M. Haque, S.S. Ray, D.J. Stuehr, Phosphorylation controls endothelial nitric-oxide synthase by regulating its conformational dynamics, J. Biol. Chem. 291 (44) (2016) 23047–23057.

[19] S. Beaumel, A. Picciocchi, F. Debeurme, C. Vives, A.M. Hesse, M. Ferro, D. Grunwald, H. Stieglitz, P. Thepchatri, S.M.E. Smith, F. Fieschi, M.J. Stasia, Down-regulation of NOX2 activity in phagocytes mediated by ATM-kinase dependent phosphorylation, Free Radic. Biol. Med. 113 (2017) 1–15.

[20] S. Rigutto, C. Hoste, H. Grasberger, M. Milenkovic, D. Communi, J.E. Dumont, B. Corvilain, F. Miot, X. De Deken, Activation of dual oxidases Duox1 and Duox2: differential regulation mediated by camp-dependent protein kinase and protein kinase C-dependent phosphorylation, J. Biol. Chem. 284 (11) (2009) 6725–6734.

[21] Y. Zhang, V. Brovkovych, S. Brovkovych, F. Tan, B.S. Lee, T. Sharma, R.A. Skidgel, Dynamic receptor-dependent activation of inducible nitric-oxide synthase by ERK-mediated phosphorylation of Ser745, J. Biol. Chem. 282 (44) (2007) 32453–32461.

[22] P.M. Bauer, D. Fulton, Y.C. Boo, G.P. Sorescu, B.E. Kemp, H. Jo, W.C. Sessa, Compensatory phosphorylation and protein-protein interactions revealed by loss of function and gain of function mutants of multiple serine phosphorylation sites in endothelial nitric-oxide synthase, J. Biol. Chem. 278 (17) (2003) 14841–14849.

[23] P. Gao, S.H. Yoo, K.J. Lee, C. Rosensweig, J.S. Takahashi, B.P. Chen, C.B. Green, Phosphorylation of the cryptochrome 1 C-terminal tail regulates circadian period length, J. Biol. Chem. 288 (49) (2013) 35277–35286.

[24] L. Fang, Z. Yang, J. Zhou, J.Y. Tung, C.D. Hsiao, L. Wang, Y. Deng, P. Wang, J. Wang, M.H. Lee, Circadian clock gene CRY2 degradation is involved in chemoresistance of colorectal cancer, Mol. Cancer Ther. 14 (6) (2015) 1476–1487.

[25] Y. Harada, M. Sakai, N. Kurabayashi, T. Hirota, Y. Fukada, Ser-557-phosphorylated mCRY2 is degraded upon synergistic phosphorylation by glycogen synthase kinase-3 beta, J. Biol. Chem. 280 (36) (2005) 31714–31721.

[26] A. Zhou, K. Lin, S. Zhang, Y. Chen, N. Zhang, J. Xue, Z. Wang, K.D. Aldape, K. Xie, J.R. Woodgett, S. Huang, Nuclear GSK3beta promotes tumorigenesis by phosphorylating KDM1A and inducing its deubiquitylation by USP22, Nat. Cell Biol. 18 (9) (2016) 954–966.

[27] Z. Wang, M. Fan, D. Candas, T.Q. Zhang, L. Qin, A. Eldridge, S. Wachsmann-Hogiu, K.M. Ahmed, B.A. Chromy, D. Nantajit, N. Duru, F. He, M. Chen, T. Finkel, L.S. Weinstein, J.J. Li, Cyclin B1/Cdk1 coordinates mitochondrial respiration for cell-cycle G2/M progression, Dev. Cell 29 (2) (2014) 217–232.

[28] M.I. Lin, D. Fulton, R. Babbitt, I. Fleming, R. Busse, K.A. Pritchard Jr., W.C. Sessa, Phosphorylation of threonine 497 in endothelial nitric-oxide synthase coordinates the coupling of L-arginine metabolism to efficient nitric oxide production, J. Biol. Chem. 278 (45) (2003) 44719–44726.

[29] X. Cao, L. Rui, P.R. Pennington, J. Chlan-Fourney, Z. Jiang, Z. Wei, X.M. Li, D.E. Edmondson, D.D. Mousseau, Serine 209 resides within a putative p38(MAPK) consensus motif and regulates monoamine oxidase-A activity, J. Neurochem. 111 (1) (2009) 101–110.

[30] X. Li, S. Nai, Y. Ding, Q. Geng, B. Zhu, K. Yu, W.G. Zhu, M.Q. Dong, X.D. Su, X. Xu, J. Li, Polo-like kinase 1 (PLK1)-dependent phosphorylation of methylenetetrahydrofolate reductase (MTHFR) regulates replication via histone methylation, Cell Cycle 16 (20) (2017) 1933–1942.

[31] J. Feng, G. Xu, J. Liu, N. Zhang, L. Li, J. Ji, J. Zhang, L. Zhang, G. Wang, X. Wang, J. Tan, B. Huang, J. Lu, Y. Zhang, Phosphorylation of LSD1 at Ser112 is crucial for its function in induction of EMT and metastasis in breast cancer, Breast Cancer Res. Treat. 159 (3) (2016) 443–456.

[32] B. Peng, J. Wang, Y. Hu, H. Zhao, W. Hou, H. Zhao, H. Wang, J. Liao, X. Xu, Modulation of LSD1 phosphorylation by CK2/WIP1 regulates RNF168-dependent 53BP1 recruitment in response to DNA damage, Nucleic Acids Res. 43 (12) (2015) 5936–5947.

[33] D. Siegel, D.D. Dehn, S.S. Bokatzian, K. Quinn, D.S. Backos, A. Di Francesco, M. Bernier, N. Reisdorph, R. de Cabo, D. Ross, Redox modulation of NQO1, PLoS One 13 (1) (2018), e0190717.

[34] A. Anwar, D. Siegel, J.K. Kepa, D. Ross, Interaction of the molecular chaperone Hsp70 with human NAD(P)H:quinone oxidoreductase 1, J. Biol. Chem. 277 (16) (2002) 14060–14067.

[35] O. Moscovitz, P. Tsvetkov, N. Hazan, I. Michaelevski, H. Keisar, G. Ben-Nissan, Y. Shaul, M. Sharon, A mutually inhibitory feedback loop between the 20S proteasome and its regulator, NQO1, Mol. Cell 47 (1) (2012) 76–86.

[36] G. Ben-Nissan, M. Sharon, Regulating the 20S proteasome ubiquitin-independent degradation pathway, Biomol. Ther. 4 (3) (2014) 862–884.

[37] D. Siegel, D.L. Gustafson, D.L. Dehn, J.Y. Han, P. Boonchoong, L.J. Berliner, D. Ross, NAD(P)H:quinone oxidoreductase 1: role as a superoxide scavenger, Mol. Pharmacol. 65 (5) (2004) 1238–1247.

[38] D. Ross, D. Siegel, Functions of NQO1 in cellular protection and CoQ10 metabolism and its potential role as a redox sensitive molecular switch, Front. Physiol. 8 (2017) 595.

[39] D. Ross, D. Siegel, NQO1 in protection against oxidative stress, Curr. Opin. Toxicol. 7 (2018) 67–72.

[40] A. L. Pey, C. F. Megarity, E. Medina-Carmona, D. J. Timson, Natural small molecules as stabilizers and activators of cancer-associated NQO1 polymorphisms, Curr. Drug Targets 17 (13) (2016) 1506–1514.

[41] I. Betancor-Fernandez, D.J. Timson, E. Salido, A.L. Pey, Natural (and unnatural) small molecules as pharmacological chaperones and inhibitors in cancer, Handb. Exp. Pharmacol. 45 (2018) 345–383.

[42] A.T. Dinkova-Kostova, P. Talalay, NAD(P)H:quinone acceptor oxidoreductase 1 (NQO1), a multifunctional antioxidant enzyme and exceptionally versatile cytoprotector, Arch. Biochem. Biophys. 501 (1) (2010) 116–123.

[43] B. Lajin, A. Alachkar, The NQO1 polymorphism C609T (Pro187Ser) and cancer susceptibility: a comprehensive meta-analysis, Br. J. Cancer 109 (5) (2013) 1325–1337.

[44] I. Lastres-Becker, A.J. Garcia-Yague, R.H. Scannevin, M.J. Casarejos, S. Kugler, A. Rabano, A. Cuadrado, Repurposing the NRF2 activator dimethyl fumarate as therapy against synucleinopathy in Parkinson's disease, Antioxid. Redox Signal. 25 (2) (2016) 61–77.

[45] J.L. Moran, D. Siegel, D. Ross, A potential mechanism underlying the increased susceptibility of individuals with a polymorphism in NAD(P)H:quinone oxidoreductase 1 (NQO1) to benzene toxicity, Proc. Natl. Acad. Sci. U. S. A. 96 (14) (1999) 8150–8155.

[46] E. Medina-Carmona, J.L. Neira, E. Salido, J.E. Fuchs, R. Palomino-Morales, D.J. Timson, A.L. Pey, Site-to-site interdomain communication may mediate different loss-of-function mechanisms in a cancer-associated NQO1 polymorphism, Sci. Rep. 7 (2017), 44352. .

[47] W.D. Lienhart, V. Gudipati, M.K. Uhl, A. Binter, S.A. Pulido, R. Saf, K. Zangger, K. Gruber, P. Macheroux, Collapse of the native structure caused by a single amino acid exchange in human NAD(P)H:quinone oxidoreductase(1.), FEBS J. 281 (20) (2014) 4691–4704.

[48] S. Chen, P.S. Deng, J.M. Bailey, K.M. Swiderek, A two-domain structure for the two subunits of NAD(P)H:quinone acceptor oxidoreductase, Protein Sci. 3 (1) (1994) 51–57.

[49] M. Faig, M.A. Bianchet, P. Talalay, S. Chen, S. Winski, D. Ross, L.M. Amzel, Structures of recombinant human and mouse NAD(P)H:quinone oxidoreductases: species comparison and structural changes with substrate binding and release, Proc. Natl. Acad. Sci. U. S. A. 97 (7) (2000) 3177–3182.

[50] R. Li, M.A. Bianchet, P. Talalay, L.M. Amzel, The three-dimensional structure of NAD(P)H:quinone reductase, a flavoprotein involved in cancer chemoprotection and chemotherapy: mechanism of the two-electron reduction, Proc. Natl. Acad. Sci. U. S. A. 92 (19) (1995) 8846–8850.

[51] A.L. Pey, C.F. Megarity, D.J. Timson, FAD binding overcomes defects in activity and stability displayed by cancer-associated variants of human NQO1, Biochim. Biophys. Acta 1842 (11) (2014) 2163–2173.

[52] I.G. Munoz, B. Morel, E. Medina-Carmona, A.L. Pey, A mechanism for cancer-associated inactivation of NQO1 due to P187S and its reactivation by the consensus mutation H80R, FEBS Lett. 591 (2017) 2826–2835.

[53] E. Medina-Carmona, R.J. Palomino-Morales, J.E. Fuchs, E. Padín-Gonzalez, N. Mesa-Torres, E. Salido, D.J. Timson, A.L. Pey, Conformational dynamics is key to understanding loss-of-function of NQO1 cancer-associated polymorphisms and its correction by pharmacological ligands, Sci. Rep. 6 (2016) 20331.

[54] W.D. Lienhart, E. Strandback, V. Gudipati, K. Koch, A. Binter, M.K. Uhl, D.M. Rantasa, B. Bourgeois, T. Madl, K. Zangger, K. Gruber, P. Macheroux, Catalytic competence, structure and stability of the cancer-associated R139W variant of the human NAD(P)H:quinone oxidoreductase 1 (NQO1), FEBS J. 284 (2017) 1233–1245.

[55] D. Siegel, A. Anwar, S.L. Winski, J.K. Kepa, K.L. Zolman, D. Ross, Rapid polyubiquitination and proteasomal degradation of a mutant form of NAD(P)H:quinone oxidoreductase 1, Mol. Pharmacol. 59 (2) (2001) 263–268.

[56] R.D. Traver, D. Siegel, H.D. Beall, R.M. Phillips, N.W. Gibson, W.A. Franklin, D. Ross, Characterization of a polymorphism in NAD(P)H: quinone oxidoreductase (DT-diaphorase), Br. J. Cancer 75 (1) (1997) 69–75.

[57] D. Siegel, S.M. McGuinness, S.L. Winski, D. Ross, Genotype-phenotype relationships in studies of a polymorphism in NAD(P)H:quinone oxidoreductase 1, Pharmacogenetics 9 (1) (1999) 113–121.

[58] E. Medina-Carmona, J.E. Fuchs, J.A. Gavira, N. Mesa-Torres, J.L. Neira, E. Salido, R. Palomino-Morales, M. Burgos, D.J. Timson, A.L. Pey, Enhanced vulnerability of

human proteins towards disease-associated inactivation through divergent evolution, Hum. Mol. Genet. 26 (2017) 3531–3544.
[59] G. Neuberger, G. Schneider, F. Eisenhaber, pkaPS: prediction of protein kinase a phosphorylation sites with the simplified kinase-substrate binding model, Biol. Direct 2 (2007) 1.
[60] J. Schymkowitz, J. Borg, F. Stricher, R. Nys, F. Rousseau, L. Serrano, The FoldX web server: an online force field, Nucleic Acids Res. 33 (Web Server issue) (2005) W382–W388.
[61] J. Van Durme, J. Delgado, F. Stricher, L. Serrano, J. Schymkowitz, F. Rousseau, A graphical interface for the FoldX forcefield, Bioinformatics 27 (12) (2011) 1711–1712.
[62] R. Fraczkiewicz, W. Braun, Exact and efficient analytical calculation of the accessible surface areas and their gradients for macromolecules, J. Comput. Chem. 19 (1998) 319–333.
[63] G. Asher, O. Dym, P. Tsvetkov, J. Adler, Y. Shaul, The crystal structure of NAD(P)H quinone oxidoreductase 1 in complex with its potent inhibitor dicoumarol, Biochemistry 45 (20) (2006) 6372–6378.
[64] R.D. Traver, T. Horikoshi, K.D. Danenberg, T.H. Stadlbauer, P.V. Danenberg, D. Ross, N.W. Gibson, NAD(P)H:quinone oxidoreductase gene expression in human colon carcinoma cells: characterization of a mutation which modulates DT-diaphorase activity and mitomycin sensitivity, Cancer Res. 52 (4) (1992) 797–802.
[65] A.L. Pey, Biophysical and functional perturbation analyses at cancer-associated P187 and K240 sites of the multifunctional NADP(H):quinone oxidoreductase 1, Int. J. Biol. Macromol. 118 (2018) 1912–1923.
[66] F.N. Barrera, M.T. Garzon, J. Gomez, J.L. Neira, Equilibrium unfolding of the C-terminal SAM domain of p73, Biochemistry 41 (18) (2002) 5743–5753.
[67] J.L. Neira, P. Sevilla, F. Garcia-Blanco, The C-terminal sterile alpha motif (SAM) domain of human p73 is a highly dynamic protein, which acquires high thermal stability through a decrease in backbone flexibility, Phys. Chem. Chem. Phys. 14 (29) (2012) 10308–10323.
[68] M.J. Abraham, T. Murtola, R. Schulz, S. Páli, J.C. Smith, B. Hess, J. Lindahl, GROMACS: high performance molecular simulations through multi-level parallelism from laptops to supercomputers, SoftwareX 1-2 (2015) 19–25.
[69] W. Humphrey, A. Dalke, K. Schulten, VMD: visual molecular dynamics, J. Mol. Graph. 14 (1) (1996) (33–8, 27–8).
[70] K. Lindorff-Larsen, S. Piana, K. Palmo, P. Maragakis, J.L. Klepeis, R.O. Dror, D.E. Shaw, Improved side-chain torsion potentials for the Amber ff99SB protein force field, Proteins 78 (8) (2010) 1950–1958.
[71] J. Wang, R.M. Wolf, J.W. Caldwell, P.A. Kollman, D.A. Case, Development and testing of a general amber force field, J. Comput. Chem. 25 (9) (2004) 1157–1174.
[72] W.L. Jorgensen, J. Chandrasekhar, J.D. Madura, R.W. Impey, M.L. Klein, Comparison of simple potential functions for simulating liquid water, J. Chem. Phys. 79 (1983) 926–935.
[73] B. Rizzuti, R. Bartucci, L. Sportelli, R. Guzzi, Fatty acid binding into the highest affinity site of human serum albumin observed in molecular dynamics simulation, Arch. Biochem. Biophys. 579 (2015) 18–25.
[74] S. Evoli, D.L. Mobley, R. Guzzi, B. Rizzuti, Multiple binding modes of ibuprofen in human serum albumin identified by absolute binding free energy calculations, Phys. Chem. Chem. Phys. 18 (47) (2016) 32358–32368.
[75] N. Mesa-Torres, I. Betancor-Fernández, E. Oppici, B. Cellini, E. Salido, A.L. Pey, Evolutionary divergent suppressor mutations in conformational diseases, Gene 9 (2018), E352.
[76] A. Jorge-Finnigan, R. Kleppe, K. Jung-Kc, M. Ying, M. Marie, I. Rios-Mondragon, M.F. Salvatore, J. Saraste, A. Martinez, Phosphorylation at serine 31 targets tyrosine hydroxylase to vesicles for transport along microtubules, J. Biol. Chem. 292 (34) (2017) 14092–14107.
[77] F.F. Miranda, K. Teigen, M. Thorolfsson, R.M. Svebak, P.M. Knappskog, T. Flatmark, A. Martinez, Phosphorylation and mutations of Ser(16) in human phenylalanine hydroxylase. Kinetic and structural effects, J. Biol. Chem. 277 (43) (2002) 40937–40943.
[78] A. Guerra-Castellano, I. Diaz-Moreno, A. Velazquez-Campoy, M.A. De la Rosa, A. Diaz-Quintana, Structural and functional characterization of phosphomimetic mutants of cytochrome c at threonine 28 and serine 47, Biochim. Biophys. Acta 1857 (4) (2016) 387–395.
[79] A. Guerra-Castellano, A. Diaz-Quintana, B. Moreno-Beltran, J. Lopez-Prados, P.M. Nieto, W. Meister, J. Staffa, M. Teixeira, P. Hildebrandt, M.A. De la Rosa, I. Diaz-Moreno, Mimicking tyrosine phosphorylation in human cytochrome c by the evolved tRNA synthetase technique, Chemistry 21 (42) (2015) 15004–15012.
[80] R. Claveria-Gimeno, A. Velazquez-Campoy, A.L. Pey, Thermodynamics of cooperative binding of FAD to human NQO1: implications to understanding cofactor-dependent function and stability of the flavoproteome, Arch. Biochem. Biophys. 636 (2017) 17–27.
[81] G. Asher, J. Lotem, R. Kama, L. Sachs, Y. Shaul, NQO1 stabilizes p53 through a distinct pathway, Proc. Natl. Acad. Sci. U. S. A. 99 (5) (2002) 3099–3104.
[82] G. Asher, P. Tsvetkov, C. Kahana, Y. Shaul, A mechanism of ubiquitin-independent proteasomal degradation of the tumor suppressors p53 and p73, Genes Dev. 19 (3) (2005) 316–321.
[83] A. Anwar, D. Dehn, D. Siegel, J.K. Kepa, L.J. Tang, J.A. Pietenpol, D. Ross, Interaction of human NAD(P)H:quinone oxidoreductase 1 (NQO1) with the tumor suppressor protein p53 in cells and cell-free systems, J. Biol. Chem. 278 (12) (2003) 10368–10373.
[84] A.C. Leney, D. El Atmioui, W. Wu, H. Ovaa, A.J.R. Heck, Elucidating crosstalk mechanisms between phosphorylation and O-GlcNAcylation, Proc. Natl. Acad. Sci. U. S. A. 114 (35) (2017) E7255–E7261.
[85] A. Cristobal, H.W.P. van den Toorn, M. van de Wetering, H. Clevers, A.J.R. Heck, S. Mohammed, Personalized proteome profiles of healthy and tumor human colon organoids reveal both individual diversity and basic features of colorectal cancer, Cell Rep. 18 (1) (2017) 263–274.
[86] M.S. Robles, S.J. Humphrey, M. Mann, Phosphorylation is a central mechanism for circadian control of metabolism and physiology, Cell Metab. 25 (1) (2017) 118–127.
[87] R. Aebersold, M. Mann, Mass-spectrometric exploration of proteome structure and function, Nature 537 (7620) (2016) 347–355.
[88] D. Wang, N. Kon, G. Lasso, L. Jiang, W. Leng, W.G. Zhu, J. Qin, B. Honig, W. Gu, Acetylation-regulated interaction between p53 and SET reveals a widespread regulatory mode, Nature 538 (7623) (2016) 118–122.
[89] S. Vega, O. Abian, A. Velazquez-Campoy, On the link between conformational changes, ligand binding and heat capacity, Biochim. Biophys. Acta 1860 (2016) 868–878.
[90] T. Cresteil, A.K. Jaiswal, High levels of expression of the NAD(P)H:quinone oxidoreductase (NQO1) gene in tumor cells compared to normal cells of the same origin, Biochem. Pharmacol. 42 (5) (1991) 1021–1027.
[91] K.A. Nolan, H. Zhao, P.F. Faulder, A.D. Frenkel, D.J. Timson, D. Siegel, D. Ross, T.R. Burke, Jr, I.J. Stratford, R.A. Bryce, Coumarin-based inhibitors of human NAD(P)H: quinone oxidoreductase-1. Identification, structure-activity, off-target effects and in vitro human pancreatic cancer toxicity, J. Med. Chem. 50 (25) (2007) 6316–6325.
[92] J.J. Cullen, M.M. Hinkhouse, M. Grady, A.W. Gaut, J. Liu, Y.P. Zhang, C.J. Weydert, F.E. Domann, L.W. Oberley, Dicumarol inhibition of NADPH:quinone oxidoreductase induces growth inhibition of pancreatic cancer via a superoxide-mediated mechanism, Cancer Res. 63 (17) (2003) 5513–5520.
[93] A.M. Lewis, M. Ough, M.M. Hinkhouse, M.S. Tsao, L.W. Oberley, J.J. Cullen, Targeting NAD(P)H:quinone oxidoreductase (NQO1) in pancreatic cancer, Mol. Carcinog. 43 (4) (2005) 215–224.